Investigating degradation pathways in organic solar cell materials

by

Satvik Shah

A dissertation submitted to the graduate faculty

in partial fulfillment of the requirements for the degree of

DOCTOR OF PHILOSOPHY

Major: Electrical Engineering

Program of Study Committee:

Rana Biswas, Co-major Professor
Vikram Dalal, Co-major Professor
Ruth Shinar
Mani Mina
Arka Ghosh

The student author, whose presentation of the scholarship herein was approved by the program of study committee, is solely responsible for the content of this dissertation. The Graduate College will ensure this dissertation is globally accessible and will not permit alterations after a degree is conferred.

Iowa State University

Ames, Iowa

2018

TABLE OF CONTENTS

ACKNOWLEDGMENTS

I sincerely thank Dr. Rana Biswas and Dr. Vikram Dalal for consistently guiding me in multiple ways throughout the course of my PhD.

I thank Mr. Max Noack and Dr. Wai Leung, Dr. Thomas Koschny, Dr. Joong-mok Park for technical education and guidance.

I thank my seniors Dr. Joydeep Bhattacharya, Dr. Pranav Joshi, Dr. Ranjith Kothhokaran, Dr. Deepak Chakroborty for inspiration and help with details of work. I thank Dr. Akshit Peer, Dr. Hisham Abbas, Dr. Liang Zhang, Mr. Behrang Bagheri, Dr. Istiaque Hossain, Mr. Harshwardhan Gaonkar for help and support with work as well as for being excellent co-workers.

ABSTRACT

Thin film organic solar is a recent technology with tremendous potential – low cost materials, quicker manufacturing processes and synthetic tuning of organic materials to optimize material properties. Cell efficiencies > 12% have already been achieved. But the bottleneck problem this technology faces is instability. Performance of these cells degrades much faster than traditional solar cells. The degradation occurs on exposure to solar radiation, both through extrinsic ingress of moisture and oxygen as well as intrinsic degradation mechanisms.

One of the most common type or thin film organic cell with efficiency ~10% is PTB7:PCBM organic solar cell. Hence I have tried to attack the instability problem for this cell. The first step is to understand why and how the degradation occurs. Hence I have studied both extrinsic and intrinsic degradation pathways for this cell. Through theoretical simulations using quantum mechanical methods, I have tried to calculate energy barriers for possible degradation pathways, narrowing their search. Next, I try to determine the atomistic mechanisms of degradation by light-soaking organic films in controlled environment and performing infrared spectroscopy before and after light soaking, to identify bonding changes. Infrared spectroscopy paired with ab-initio theoretical modeling can provide a powerful tool for quantifying photo-structural atomic bonding changes.

Understanding these pathways, it will be easier to synthetically tune organic materials much less prone to degradation, solving the bottleneck problem of instability for thin film organic solar cells and opening avenues to designing more stable organic materials for organic electronics.

CHAPTER 1. INTRODUCTION

1.1 Motivation

This work aims at a fundamental understanding of the chemical degradation processes of organic solar cell materials.

Organic solar cells (OSCs) are inexpensive due to bulk fabrication processes and their efficiencies have been increasing over the past decade. But they face the strong bottleneck problem of degradation. However, the organic materials that make OSCs have an almost infinite potential to be synthetically tuned to modify their properties. Can we make organic materials for these cells that overcome the degradation bottleneck?

There have been few studies that explore in detail the chemical degradation mechanisms of these materials. We have tried to understand these degradation processes both using extensive theoretical simulations using computational physics and experimental methods. For this purpose, we have used a particular OSC (PTB7:PCBM) as a prototype because a large number of OSCs can be considered as derivatives of this type hence with the hope that our results can be significantly generalized later on.

We hope that this work contributes to an increased understanding of the degradation processes of OSC materials and hence can help in the battle to overcome this bottleneck problem.

1.2 Solar Cells

A solar cell is an optical-electrical device that converts energy from sun-light to electrical energy. There are many kinds of solar cells. Different solar cells can be made of different materials,

may have different electrical contacts and come in a variety of sizes and shapes. But in spite of the observed variety in solar cells all should satisfy certain common characteristics. Solar cells are expected to absorb electromagnetic radiation with a particularly high sensitivity to the dominant spectral region in the solar spectrum. All solar cells are similarly expected to convert a maximum portion of this absorbed radiation into electrical charges of opposite polarities and to have the ability to separate these charges. Further, we must be able to collect these charges using electrical contacts, obtaining thus a continuous flow of electricity. Furthermore, solar cells are expected to deliver a more or less constant flow of electricity over long periods of time (order of 2-3 decades) to justify the energy put into their complex manufacturing process.

Fig 1. PV array made of cadmium telluride (CdTe) solar panels
[Source: https://www.nrel.gov/data/pix/Jpegs/14726.jpg]

1.3 Usage

Humanity is a massive consumer of electrical energy. We produce electrical energy in tremendous proportions every year and our usage is increasing continuously. We use this electricity both in our homes and our industries, and of its different applications, we are all too aware.

There are a variety of ways in which we produce electricity for our use, the major portion being extracted by converting coal and natural gas obtained from the earth into electricity by a complex process. But such fuels are rapidly depleting from the earth's crust, hence several other ways – wind power, hydroelectric power and solar power, to name a few – have emerged to potentially replace these older technologies when the time is ripe.

The technology of solar cells has been continuously improving and with economies of scale is increasingly becoming competitive to the traditional technologies (Table 1.1).

Table 1 **levelized energy costs** (LEC) 2016. Adapted from US DOE

Power Plant Type	Cost $/kW-hr
Coal	$0.095-0.15
Natural Gas	$0.07-0.14
Nuclear	$0.095
Wind	$0.07-0.20
Solar PV	$0.125
Solar Thermal	$0.24
Geothermal	$0.05
Biomass	$0.10
Hydro	$0.08

1.4 Working of a solar cell

In line with the processes mentioned for converting light to electrical energy (section 1.2), namely light absorption, charge generation and separation, charge carrier collection, a solar cell consists of a main layer or absorber layer, an electrical junction that can separate charge carriers and electrodes or metal contacts that form a well behaving electrical contact with the external circuit. These fundamental parts of a solar cell are illustrated in the figure 1.2.

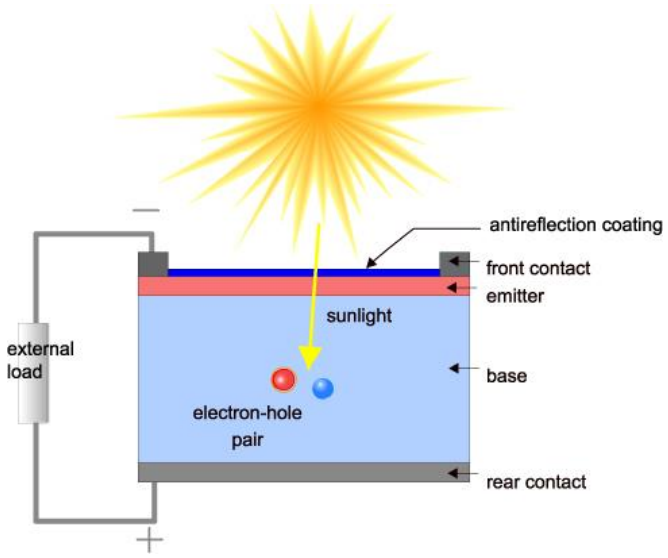

Fig 2 Schematic of a solar cell illustrating its working principle.
[Source: http://pveducation.org/pvcdrom/solar-cell-structure]

The absorber layer should be such that it can convert incident solar radiation directly into mobile electrical charges. An electrical semiconductor is precisely such a material. Incident photons having an energy greater than the bandgap of the semiconductor produce an electron-hole pair, those with energy less than the bandgap aren't absorbed at all while those with energy greater than the band gap usually produce an electron hole pair and lose part of their energy. To maximize energy conversion efficiency with respect to the solar spectrum, an ideal semiconductor should

have a bandgap of 1.34eV, putting an upper limit on the efficiency of solar cell at 35% called the Shockley-Quiesser limit.

The generated electron hole pair is called an exciton and usually requires some energy to decouple the pair. This energy is called the binding energy and is different for different absorber materials. For Silicon this is readily available at room temperature from the thermodynamic energy of atoms.

The generated charge carriers are liable to recombine inside the material unless separated by an electric field. An electrical p-n junction is used to create such a built-in electric field. Ohmic electrical contacts connect the solar cell to external circuit.

Corresponding to above mentioned processes inside a solar cell, we have a few ways to make a solar cell more cost effective - cheaper absorbing material, cheaper encapsulating material, absorber with greater absorption coefficient – less material required, photonic enhancement techniques to improve absorption, increased efficiency of solar cell measured as electrical power output produced per unit input of solar radiation.

1.5 Organic solar cells

Thin film solar cell is a comparatively recent technology having absorber layer with high absorption coefficient and hence low material requirement reducing the overall cost. But as a tradeoff, they generally tend to have lower efficiency.

The main layer materials typically used in organic solar cells have a very high absorption coefficient. Hence a very thin film of the material suffices to absorb most of the incident light. These typically use two different organic semiconductor materials and form a heterojunction so that charges can be separated.

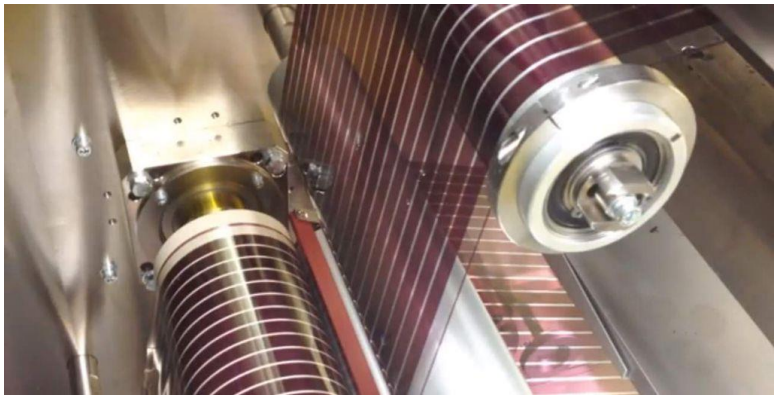

Fig 3 OSC fabricated by roll-to-roll processing.
[Source: http://cen.acs.org/content/cen/articles/94/i18/1461870023560.jpg]

These organic materials are cheap to chemically synthesize as compared to synthesizing say electronic level purity Silicon or Cadmium Selenide. Moreover, these organic compounds are soluble in certain standard organic solvents making it easy to deposit their thin films. These films can be deposited on malleable plastic sheets instead of solid substrates. Subsequently, these substrate-sheets can be mounted on a variety of places including building windows, roofs, terraces and other public places. Thus, organic solar cells can be inexpensively manufactured.

1.6 Problem re-statement

In 2013, when I started my PhD, organic thin-film solar cells were already giving good efficiencies (around 10%) and emerging as an inexpensive option to commercial established Si and CdSe technologies. One problem still remained – organic solar cells degrade. Hence I began investigating why these materials degrade. I found several broad reasons existing in literature – degradation of the material itself, of the interfaces with other materials, and external influence (of moisture or oxygen for example). This external influence could be limited by encapsulation.

The interfacial materials used in thin film organic cells were already being used in other kinds of solar cells without such pronounced degradation difficulties. Why did some of them have bad interfaces with organic materials only and not with other kinds of solar cells? We are eventually led to the deceptively simple question – why do organic materials degrade?

One of my basic hypothesis is – a fundamental and deeper understanding of organic materials from the point of view of their susceptibility to degradation would lead in future to significant improvements in designing stable organic molecules. Of course, the primary needs of high absorption, efficient charge transfer, 'good' band-gap (according to the Schockley-Queisser limit) are assumed to be already met. That is why I do not start from scratch, but look at and try to understand only organic molecules that are already used to make efficient solar cells.

1.7 Research Outline

We first turn to existing literature examining possible mechanisms for chemical degradation of PTB7. In chapter 2, using extensive theoretical simulations we find out the enthalpy change and activation energy for several possible mechanisms, increasing our understanding of the polymer and the key points which make it susceptible to degradation.

In Chapter 3, we try to explore the chemical mechanisms using the experimental tool of infrared spectroscopy. The study corroborates the large key findings in Chapter 2.

In Chapter 4, we use the same tool to understand degradation in another common organic polymer P3HT which makes more stable albeit lower efficiency OSCs.

In Chapter 5, we come up with a variant of P3HT (deuterated P3HT) which should build an OSC with similar efficiency but should have higher stability.

In Chapter 6, we try to experimentally find out the activation energy for degradation of PTB7 and compare it with values we found using theoretical simulations in Chapter 2.

CHAPTER 2. ATOMIC PATHWAYS UNDERLYING LIGHT INDUCED CHANGES IN ORGANIC SOLAR CELL MATERIALS

*Satvik Shah[1], Rana Biswas[1,2]**

1. Department of Electrical and Computer Engineering, Iowa State University, Ames, IA 50011, United States.

2. Ames Laboratory, Department of Physics & Astronomy, and Microelectronics Research Center; Iowa State University, Ames, IA 50011, United States.

KEYWORDS. Organic solar cell, light induced degradation, atomistic rearrangement

Adapted from an article published in Journal of Physical Chemistry C, **119** (35), 20265–20271 (2015)

2.1 Abstract

We identify atomic pathways, involving local O and H motion, which underlie intrinsic light-induced changes of organic materials, utilizing ab-initio simulations. Light exposure generates prolonged intrinsic degradation of organic solar cells, when moisture and oxygen are absent. We consider the polymer PTB7, common for higher efficiency cells. Local motion of Ofrom the C-O-C bridge to a C=O bond in the aromatic backbone, creates a C-dangling bond defect, with an energy of 2.1 eV. The energy barrier of ≤2.65 eV can be surmounted with blue photons. Local H motion from βC to αC within the alkyl, also generates a C-dangling bond, a similar re-bonding of bridging-O, and cleaving of PTB7. Bridging Ocreates instability. Defect

energies are lowered by ~0.5 eV by excited electronic states. Defects can anneal reversiblyor irreversibly to distorted configurations. We identify why certain organic materials are more stable, and pathways to design more stable materials.

2.2 Introduction

Organic solar cells have witnessed a very rapid rise in efficiencies from 4% just 10 years ago to 11% recently[1]. The best single junction solar cells using either narrow band gap polymer donors1or small molecule based absorbers[2] have achieved 8% power conversion efficiency. By achieving broad-band light absorption with tandem solar cell configurations[3,4] employing low and high band gap absorbers, a 11% power conversion efficiency has been achieved, making organic solar cells competitive with other thin film technologies. The critical problem in these solar cells is their stability, since the deployment and commercialization of these novel organic solar cells requires that they be *stable* in ambient outdoor light conditions.

The stability of organic solar cells (OSCs) has been studied by numerous researchers, summarized in the comprehensive reviews by Jorgensen et al[5,6]. It is well established that exposure to oxygen and moisture can rapidly degrade OSCs by an erosion of the ITO electrodes, an uptake of water by the hygroscopic PEDOT:PSS layer and its oxidative degradation, or the oxidation of the polymer absorber layer5. Organic absorber layers with vinylene groups (e.g. MEH-PPV) are particularly susceptible to oxidative degradation, whereas polymers without vinylene groups (e.g. P3HT) are substantially more stable5. The deleterious effects of oxygen and moisture can be eliminated by performing the light exposure in an environmental chamber with inert nitrogen gas flow in the laboratory (Fig. S1). We

performed controlled light exposure in an environmental chamber with nitrogen flow that demonstrated prolonged degradation of polythieno[3,4-b]-thiophene-co-benzodithiophene; [6,6]-phenyl C71 -butyric acid methyl ester (PTB7:$PC_{70}BM$) OSC's (Fig. S2), and poly(3-hexylthiophene-2,5-diyl):$PC_{60}BM$(P3HT:PCBM) OSCs (Fig. S3), accompanied bythe creation of mid-gap defect states[7] within 96 hours of exposure (Fig. S3). Street et al performed light exposure of P3HT:PCBM and poly(carbazoledithienyl-benzothiadiazole):phenyl C70-butyric acid methyl ester (PCDTBT:$PC_{70}BM$) cells and demonstrated an increase of the induced localized electronic state density near the middle of the gap[8] and a near stabilization of the defect density at long time suggesting self-annealing of defects[9]. Thermal annealing also induced increases in the band-tail defect states8. Even longer time exposure extending over 4500 hours (equivalent to ~3 years of daytime exposure), observed an initial burn-in period where polymer OSC characteristics drop nearly exponentially[10]. This was followed by a slower linear decay period that extends over much longer times[10].

These recent studies raise the central question:that even in the absence of oxygen and moisture, what is the *intrinsic* mechanism of degradation in OSCs from the light exposure alone? This question is important since *intrinsic* light degradation cannot be eliminated by encapsulation methods. Another fascinating question is whether the degradation is reversible or irreversible, an issue that has been studied in many amorphous systems.

Measurements of photo-current and cell efficiency reductions are macroscopic parameters that do not provide microscopic atomistic detail of the processes underlying the degradation. To address this question, Street, Northrup and Krusor proposed[11] that the breaking of C-H bonds resulting in the generation of a dangling bond on the C accompanied by H migration to form a H-induced CH_2 defect in the thiophene ring could account for many

features of X-ray induced degradation in P3AT (A=alkyl). By rigorous ab-initio simulations Northrup found[12] that the energy barrier that needs to be overcome for these CH_2 defects in P3AT was ~3.1 eV although the net energy cost was 1.27 – 1.35 eV. Such energy barriers or formation energies are consistent with defects induced through X-ray or UV irradiation. The concept of H release from bonded configurations, accompanied by H migration, has many analogies to the well-known Staebler-Wronski effect[13] of the reversible degradation of hydrogenated amorphous silicon (a-Si:H).

The goal of this paper is to elucidate the atomistic nature of changes leading to degradation of higher efficiency OSC's composed of the newer *lower band gap polymers* such as (PTB7). Since PTB7 based OSC's have led to the highest power conversion efficiency (>8%) single junction solar cells[14], it is important to understand photo-structural changes in PTB7 rather than in prototypical higher band gap polymers such as P3HT, which leads to considerably lower efficiency (~4%) solar cells. We focus on changes that can be induced *purelyby light exposure,* without the in-diffusion of oxygen or water which caused well known degradation effects. This sets *intrinsic* limits on the photo-stability of the OSCs. The previous work on atomistic mechanisms underlying degradation of the common P3AT/P3HT based solar cells[12] serves as a most useful guide although we find mechanisms can be very different in PTB7 due to the presence of O within the donor. OSC's with high efficiency (~8%) are composed of the intimately blended donor-acceptor (D-A) regions of PTB7-$PC_{71}BM$. Most incident photons are absorbed in the donor PTB7 forming an exciton which diffuses ~10 nm to the D-A interface, where the exciton dissociates to release a hole in the donor and electron in the acceptor. Since the light absorption and exciton motion is confined to the donor, it is valid to consider photo-structural changes in the donor only without the bonding of the nearby

acceptor, as considered by previous studies[12,15] of P3HT based OSCs. We investigate photo-structural atomistic changes with ab-initio simulations.

2.3 Simulation Methods

In this work, the Spanish Initiative for Electronic Simulations with Thousands of Atoms (SIESTA)[16] method was employed, to simulate the electronic properties of organic materials.

The *ab initio* density functional theory (DFT) with the SIESTA method utilized Troullier-Martins norm-conserving pseudo-potentials[17], in a fully non-local form, with a basis set composed of multiple-zeta pseudo atomic orbitals. The self-consistent potential was calculated on a real space grid whose spacing was determined by an energy cut-off of 100 Ry. The exchange correlation functional we used was the general gradient approximation (GGA) using the Perdew-Burke-Ernzerhof (PBE) parametrization of the exchange-correlation functional[18]to treat the nonlocal exchange and correlation energies.We obtain the electronic structure, density of states, and total energies. The local orbital based SIESTA method allows computationally efficient calculations in a multi-processor environment. The structural relaxation is performed with a steepest descent algorithm to obtain the low energy configurations.

We focus our investigations on PTB7 as a prototypical donor for organic solar cells and expect our conclusions to be valid to other donors with similar bonding characteristics. SIESTA has previously successfully described the structure and bonding of organic molecules such as pentacene[19] and is a computationally efficient method for simulating organic polymers. PTB7 consists of a planar conjugated back bone of connected thiophene groups and benzene rings (Fig. 1a). The conjugated backbone is connected to alkyl chains (Fig. 1a) through a bridging oxygen (O) and a carbon atom (α-C). PTB7 can be viewed as a combination of two

monomers TT and BDT. The highly electronegative fluorine makes the TT monomer portion electronegative, leading to a charge separation between the monomers akin to a donor-acceptor pair.

a) b)

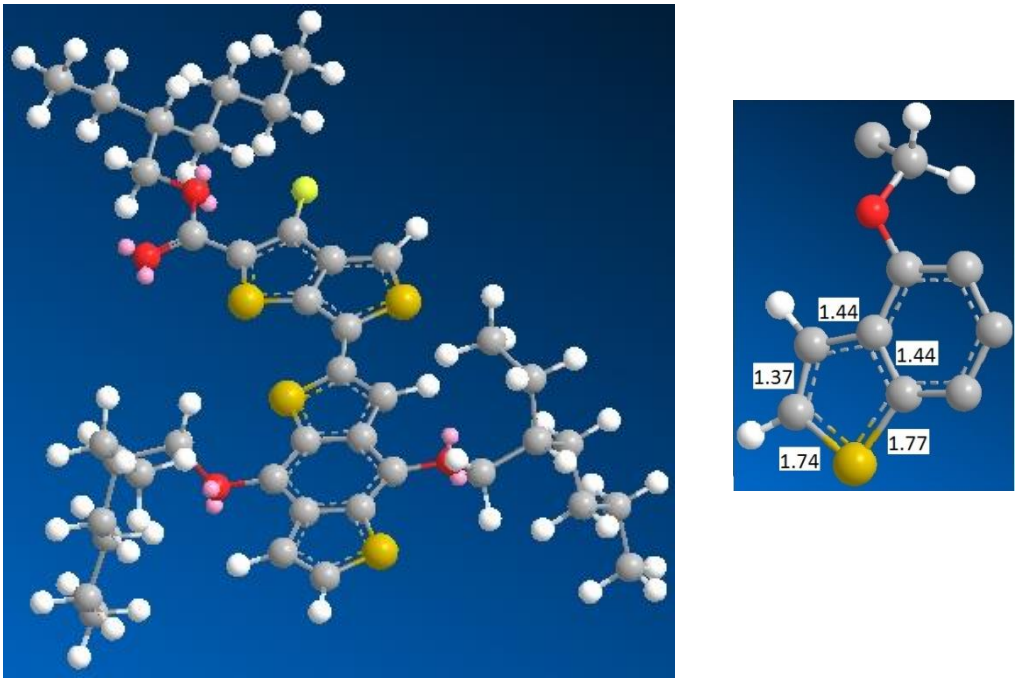

Fig. 1 a) Simulated PTB7 where C atoms are gray, H white, O red, S yellow and F yellow-green. Lone-pair electrons are identified by small pink circles. The conjugated backbone is identified with dotted lines. The conjugated backbone is connected to alkyl groups through bridging O atoms with lone pairs. As discussed in the text, H atoms are utilized to cap ends of the polymeric chain. b) Local conformation around bridging O and bond lengths within the thiophene ring.

Although PTB7 is a polymer we adopted a 105-atom segment of the PTB7 chain for our investigations by capping the ends of the conjugated segment with H atoms. This permitted the use of a simulation cell of dimension (2.41 nm x 2.15 nm x 1.35 nm) with periodic boundary conditions. These cell dimensions were adopted so that a vacuum region exceeding 1 nm

separated the PTB7 structure from its periodic images, effectively isolating the electronic properties of each cell. The HOMO-LUMO energy level splitting is 1.54 eV, slightly lower the experimental value of 1.63 eV[20]. The underestimation of band gaps with density functional methods is considerably improved with GGA and the PBE exchange correlation functional.

SIESTA produces relaxed bond lengths within the thiophene ring (Fig. 1b) as 1.43Å for the C-C bonds, 1.7 Å for C-S, and 1.53 Å for C-H that are in good agreement with values from the literature. C-H bond lengths in the alkyl chain are 1.53 Å.

2.4 Results

We investigate the fundamental atomistic mechanisms underlying degradation in the prototypical organic donor PTB7. Our approach is to identify structural rearrangements of the PTB7 polymer that have low energy, and can be reached *without altering* the atomic constituents or number of atoms, as would be expected for photo-induced changes. We preclude in the present analysis conformational changes that are caused by addition of external species such as O_2 or water, when PTB7 is exposed to the atmosphere. PTB7 has O atoms that are not present in P3HT, making mechanisms of degradation more complex in PTB7 than the previously studied P3HT12. We examine re-bonding of both H and O atoms within PTB7. Our central result is that we identify *two* low energy structural rearrangements of PTB7, one accessed by O release followed by local O-motion, and the other by H-release and local H-motion and re-bonding. In both cases, the bridging O atom is involved and new C=O double bonds are formed. Our photo-induced conformational changes are expected to be neither exhaustive nor complete for such a complex polymer, but should be representative of structural changes and degradation pathways in this class of organic polymers.

PTB7 can be visualized as an aromatic backbone connected to O which is bonded to the α–C atom (Fig. 1b). The α–C is singly bonded to the β–C atom. The β-C forms part of the alkyl chain, with C-C single bonds at the β-C site. As we move further away from the aromatic backbone the C atoms decrease in reactivity, resulting in the highest reactivity for α–C followed by β-C. Since alkyl chains are connected to each of the bridging O atoms, it suffices to consider just one of the alkyl chains and schematically the PTB7 bonding can be represented by alkyl- βCH – αCH_2 – O – (aromatic backbone) .

2.4.1 O-induced defect formation

We find a pathway for photo-induced defect formation that is driven by local motion of the bridging O atom that connects the aromatic backbone to the alkyl chain (Fig. 2a). In the first step the O atom is released from its bridge bonded site between the α–C and C' atom (of the aromatic backbone) and moves towards C', away from α–C. In the defect state (Fig. 2b) the O is bonded to C' with a C'=O double bond length 1.29 Å. In this intermediate state α–C and C' are bonded very weakly with a bond length of 1.73 Å (Fig. 2b), so that α–C is effectively 3-bonded with a dangling bond, and PTB7 is ruptured. The site C' is nearly 4-coordinated (with bond lengths 1.48 Å, 1.53Å and 1.29Å (C=O), in addition to the weak α–C-C' bond. The PTB7 backbone loses aromatic character (Fig. 2b) within the benzene ring. The energy of this defect is 2.17 eV, and is significantly smaller than the C-C bond energy of 3.3 eV, due to the formation of the weak α–C-C' bond. There is also energy gain of ~0.28 eV from the conversion of 2 C-O bonds (with energy 3.71 eV) into a C=O double bond with energy 7.7 eV. The defect state can be annealed to low energy states (Fig. 2c, Fig. 2d) as discussed later.

In this defective intermediate state (Fig. 2b) there are two energy levels within the energy band gap (Fig. 2e) in between the LUMO and HOMO levels of PTB7. This agrees very well with the measured increased of defect densities within the gap, after light soaking7. Although we have calculated the energy of the defect in the electronic ground state, such defects are formed by photo-excitation of an e- to the LUMO level (-2.18 eV, Fig. 2e). This e- can transition downward to the LUMO level of the defect (-2.74 eV), for an energy gain of 0.56 eV, suggesting a defect energy of E'~1.61 eV for the excited electronic state (Fig. 2). The lowering of energies and energy barriers in excited electronic states is well known from previous first-principles computations[21,22]. The defect formation involves breaking of the αC-O bond (with bond energy 3.71 eV), with simultaneous formation of a weak αC-C' bond and C=O double bond.

We estimated energy barriers by linearly varying the position of all atoms between their initial ($\mathbf{R}_i$) and final positions ($\mathbf{R}_f$), so that $\mathbf{R}(\beta)=\mathbf{R}_i+\beta\mathbf{R}_f$, with a single reaction coordinate β ($0<\beta<1$). For each β the atoms αC-C' were kept fixed and other atoms were relaxed. In a second relaxation step the αC and C' were relaxed keeping the remaining atoms fixed. This two-step procedure yielded the highest energy barrier of ~2.68 eV for the intermediate value of $\beta=0.6$ (Fig. 3).

Such energy barriers can be surmounted by blue photons of wavelength 468 nm. Our calculated energy barrier is an *upper limit* to the actual energy barrier, since more complex configurational paths can be accessed, and it is reasonable to expect energy barriers of a few tenths of an eV lower, which may then be surmounted with green photons. Further computational methods are needed to estimate such complex energy barriers.

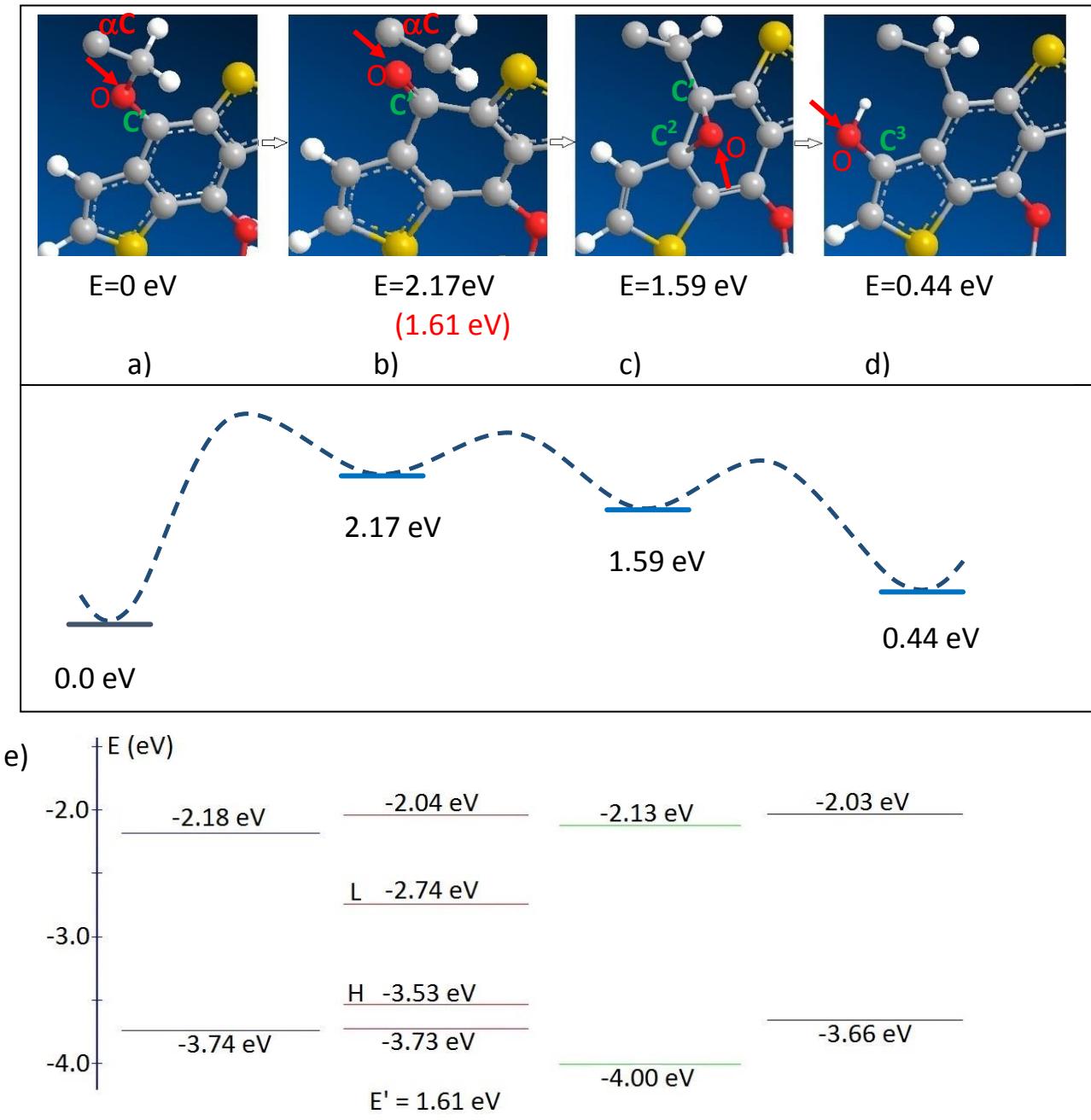

Fig. 2. Low energy structural change involving motion of O atom (red) -that connects the aromatic backbone t the alkyl chain. a) The O between the αC and C' atom connected to the aromatic back bone of the initial state (left panel) is released. b) O is bonded to the C' forming a C=O. c) In an annealing step the O can move further forming a C'-O-C^2 bridge. d) The O atoms moves to bond to the C_3 atom of the thiophene ring forming a new O bond and an O-H bond. The schematic configurational surface between the configurations is shown. e) Electronic energy levels with LUMO (L) and HOMO (H) labeled for the defect.f) Computed energy barrier between configurations in a) and b)

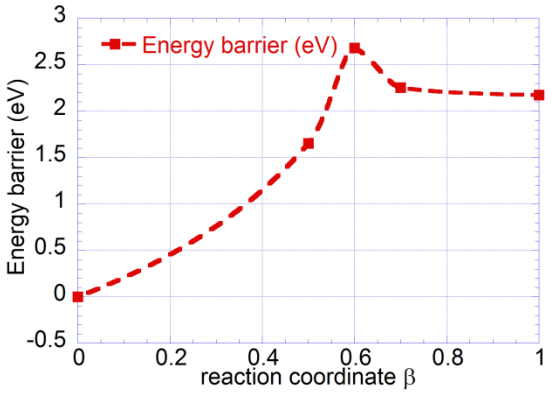

Fig. 3 Computed energy barrier between initial configuration (Fig. 2a) and defect (Fig. 2b) as a function of the reaction coordinate.

We find that this defective state can be annealed by returning to the initial state through motion of the O back to the bridging site between α-C and C'. The annealing can also be affected by further motion of the O towards the thiophene ring. The O can form a bridge bond between C^2 and $C^1$with elongated bond lengthsof 1.43 Å and 1.45 Å (Fig. 2c). The energy of the intermediate defect state is 1.59 eV and the aromatic character of the backbone is lost. Finally, the O can move further towards the C^3 site of the thiophene. The C^3-H bond is broken and the C^3-O-H bond is formed. Equivalently the O inserts into the C^3-H bond on the thiophene ring, forming a hydroxyl group. The aromatic character of the backbone is preserved with the formation of a C-O-H on the thiophene instead of the C-H. The structural change is schematically C^1-O-C' +H-C^3(thiophene) $\rightarrow$ C^1-C' + H-O-C^3(thiophene).

We find the final configuration to have a very low energy (~0.44 eV) above the initial configuration, with no defect levels in the gap (Fig. 2e), and view it as distorted PTB7. The structural change from the defect (Fig. 2b) to the thiophene distorted PTB7 (Fig. 2d) is a defect annealing step.

We may rationalize the low energy of this configuration (Fig.2d) by estimating bond energies. From the initial PTB7 state (Fig. 2a) two C-O bonds (2x3.71 eV=7.42 eV) and a C-H bond (4.29 eV), are broken for an bond energy of 11.67 eV. In the final state the C-C bond (3.6 eV) and C-O (3.71 eV) and O-H (4.81 eV) are formed for an energy of 12.12 eV, *larger* than the initial state. This simple estimate suggests an energy gain of 0.45 eV from the initial state, consistent with the ab initio result, and providing a simple argument for the lower energy of the final state. It is notable that a C-O-H group characteristic of an alcohol derivative is formed.

2.4.2 H-induced bond rearrangement

In the second conformational change we focus on the portion of the alkyl chain that is bonded to the aromatic backbone (Fig. 4 a,b,c). In the *first* step H is released from the β-C atom on the alkyl chain and migrates to the α-C atom. This ruptures the α–C-O bond, leading to the formation of a trihydride on α-C, which retains 4-coordination (Fig. 4b). The O atom forms a double bond with the C' atom of the aromatic backbone (C=O with bond length 1.28 Å), and the aromatic character of the benzene group in the backbone is lost (Fig. 4b). There is a single dangling bond on the three-coordinated β-C atom of the alkyl chain. The energy of the intermediate metastable defect configuration has an energy of 2.2 eV. In the defect state the PTB7 is cleaved with the alkyl group detached from the aromatic backbone, thereby losing its ability to act as a donor. The defect state has 2 energy levels within the band gap, again in good agreement with the measured increase in DOS above the HOMO level.

We can estimate the effect of excited electronic states, similar to the previous analysis for the O-induced defect. In the excited state the electron that occupies the LUMO level of PTB7 (-2.18 eV, Fig. 4b) can transition to the LUMO level of the defect (-2.59 eV,

Fig. 4d) for an energy gain of 0.41 eV. With this energy gain, the excited state has an estimated energy of E'~1.79 eV

There are two pathways for annealing, with the defect state first having to surmount energy barriers to return to the initial PTB7 configuration (Fig. 4a). Another annealing pathway involves this metastable defective state evolving to the configuration (Fig. 4c) where the O is bridge bonded to the β-C atom, *removing* the dangling bond on β-C. The O returns to being bridge bonded between the β-C and C^1 atoms with single bonds and the aromatic character of the backbone returns. There are no broken bonds in this configuration (Fig. 4c), which is a distortion of the PTB7 polymer, with an energy 0.26 eV above the initial state.

The low energy of the final distorted configuration can be understood since it involves a transposition of a C-H bond on βC to αC, and O bridges C and βC (rather than C-αC). The C-O bonds are broken and C-C single bond altered in the initial state to form a C=C bond and O-H. (H-C-C + C-O $\rightarrow$ C=C + O-H). The initial bond energies of a single C-C bond (3.6 eV), C-H (4.25eV) and C-O (3.71 eV) add to 11.56 eV. The final C=C double bond (6.33 eV) and O-H (4.81 ev) with energy 11.14 eV. The expected energy cost is just ~0.42 eV from simple bonding estimates is consistent with the ab-intio calculation, and accounts for its low energy.

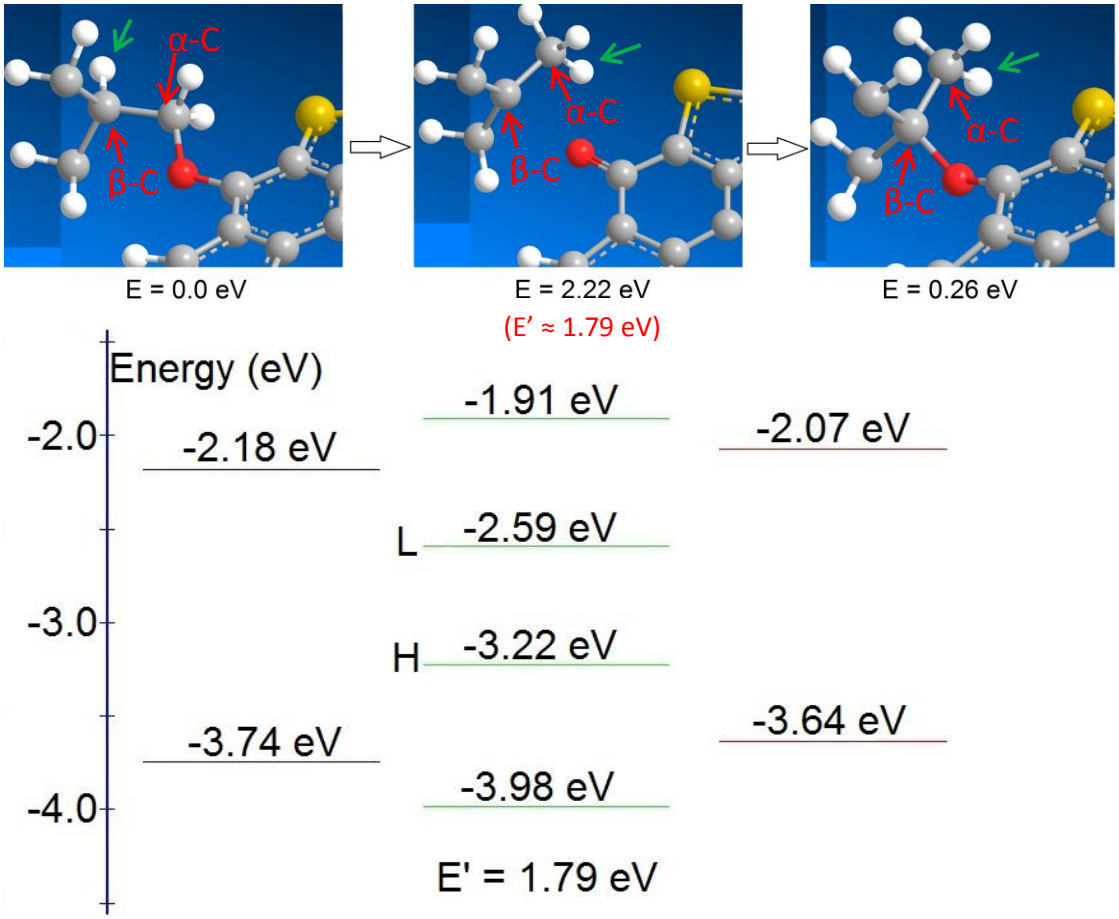

Fig. 4. Structural changes driven by motion of Hatom (at green arrow) on the alkyl chain to the neighboring C^{α} atom. a) Initial PTB7 polymer, showing portion of the alkyl group bonded to the aromatic backbone. b) In the metastable state (b) the C^{α} -O bond is broken, resulting in a a trihydride on C^{α} and a C=O double bond, and a rupture of the PTB7 polymer. c) the final low energy configuration where the O atom rebonds to the C^{β} atom on the Alkyl chain restoring aromatic character within the backbone. d) Electronic Energy levels in the three configurations.

2.4.3 H induced defects in the thiophene

We compare these two low energy configurational changes with the previously studied H-induced defects in P3AT12, where H was released from the α-C site and migrated to the thiophene ring (Fig. 5). This H bonds to a C in the closest position (position 2) to the αC site,

generating a CH_2 defect within the thiophene ring. A dangling bond is left behind on the αC site schematically represented as

(…CH..)alkyl + [--CH--]thiophene → (…C*..)alkyl + [--CH_2--]thiophene.

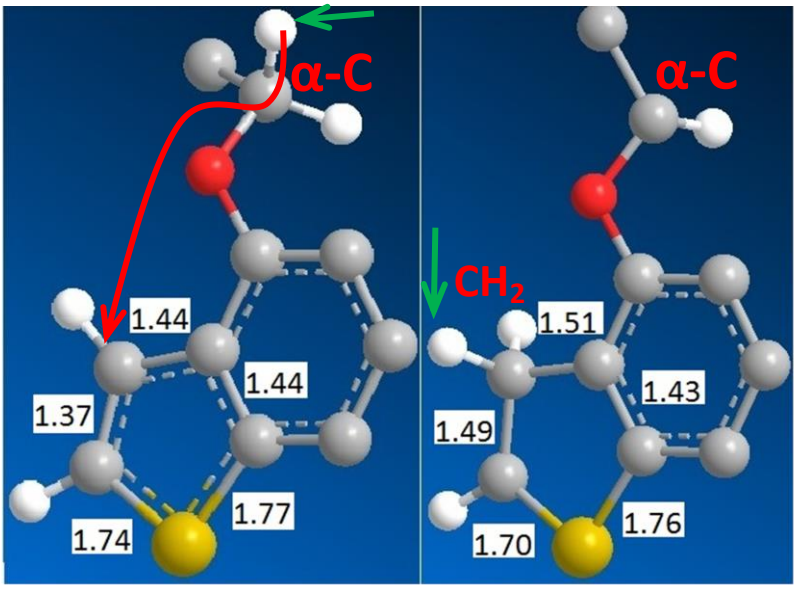

Fig. 5 Configurational change in a portion of the PTB7 polymer, showing the formation of the CH2 defect. The left panel is the initial configuration. The right panel shows motion of H from the alkyl chain to the thiophene ring. The bond-lengths are indicated in Å.

We find the energy of this defect is 3.01 eV - significantly higher than the previous two defects. Such a high energy is reasonable since the CH bond energy is 4.25 eV and is only partially recovered by the CH_2 defect of the thiophene ring. We have tested the migration of other H atoms in the alkyl chain to the thiophene ring to form the CH_2 defects and also find energies of 3.87- 3.99 eV. These high energies suggest unfavorable formation of the CH_2 defect and we have not investigated the energy barriers for this migration which are likely to be even higher. Several states are generated within the band gap, due to the dangling bond and CH_2

defect. The conjugation of the thiophene ring is lost (Fig. 4) with C-C bond lengths of 1.51 Å and 1.49 Å at the CH_2 defect substantially longer than the (1.40 Å, 1.37 Å) in the original thiophene ring but slightly shorter than that of the 1.54 Å of the C-C single bond.

2.5 Discussion

We expect light exposure to lead to structural defects such as found here. Initially the kinetics will be dominated by defect creation, that are known to cause increases of gap states, accompanied by reductions of the short circuit current and solar cell efficiency. At long illumination times, when a considerable defect density has built up, the annealing of the defects becomes important. A balance between defect creation and annealing can lead to a saturation of the defect density and a steady state value of short circuit currents and cell efficiency. As evident from Fig.2, barriers to annealing back from defect configuration (Fig. 2b) to the initial state (Fig. 2a) is ~0.5 eV. It is then possible to thermally anneal such defects at elevated temperatures. However PTB7 is not stable at elevated temperatures, thereby restricting the annealing effectiveness. Other organic donor such as P3HT are more stable at elevated temperatures and do show thermal annealing of light induced degradation[23]. However the annealing of the defect (Fig. 2b or Fig. 3b) can also lead to a channel of irreversible changes (to the structures in Fig. 2c and 2d), where the PTB7 is distorted implying that light induced degradation may only be *partially* reversible to the initial state. Depending on the magnitude of the energy barriers, different configurations (e.g. Fig. 2c, d) will coexist with the initial state (Fig. 2a) at thermal equilibrium as a result of thermal annealing. It is also conceivable that energy barriers from the defect state (Fig. 2b) to the distorted states (Fig. 2c and 2d) will be

lower than the barrier to the initial state (Fig. 2a), implying that much of the annealing would be irreversible. Kinetics of defect creation and differences in short and long-time degradation is an aspect for further work.

The defect driven local H motion in the alkyl chain (Fig. 3) has analogies to the local H-motion proposed for dangling bond creation in the Staebler-Wronski degradation of amorphous semiconductors[24]. However the re-bonding of O from C-O-C to C=O bonds here, due to the ability of C to form multiple bonds, is central to the defect formation, and is not possible in purely inorganic materials. The local motion of H here, is distinctly different from long-range H motion proposed for the Staebler-Wronski degradation in a-Si:H[25].

Our results suggest possible pathways to design more stable organic light absorbers. The bridging oxygen atom in PTB7 is a critical source of instability, and all PTBx (e.g. x=8,9) donors would be expected to have similar instability. Replacing S by Se changes band gaps[14] and solar cell characteristics, but would not be expected to have higher stability. The absence of O in P3HT together with the larger calculated energy barrier for H-motion, indicates slower degradation effects for P3HT, which agrees with observations. We anticipate ab-initio approaches can design more stable and higher efficiency designer organic polymers by utilizing band gaps and HOMO LUMO levels in addition to the structure.

Here we have considered photo-structural changes in the polymer donor PTB7. It should be noted that for planar OSC's with small molecule donors and C60-fullerene acceptors, photo-oligomerization (i.e. polymerization) of fullerenes is significant[26]. However it has been found that the C70-fullenerene base acceptors ($PC_{70}BM$) considered here, have a much lower tendency to undergo photo-oligomerization[27]. This is an aspect for further study.

The present simulations identify certain local minima in the reaction coordinates that correlate with observable mid-gap states. These local minima are by no means exhaustive and other local energy minima may well exist. An example of alternative energy minima is provided by a recent study of degradation of P3HT-PCBM organic solar cells in the dark[28] that found a gradual decrease of the efficiency from 3% to 1.5% with shelf time, and stabilization after ~1 year. The overall absorption properties of the film decreased but there was a measureable increase in the absorption in the 650 nm - 800 nm band, that was interpreted as due to the formation of localized donor-acceptor charge transfer complexes, with mid-gap states that increase recombination. We have not simulated donor-acceptor interfaces in this study or the formation of such complexes, but that is clearly an aspect for future work using atomistic models of the bulk heterojunction.

2.6 Conclusions

Our measurements on OSC's reveal prolonged intrinsic degradation of solar cell characteristics, even when solar cells were exposed in an inert environment where oxygen and moisture were absent. We identify plausible atomic origins of this *intrinsic* degradation, with ab-initio density functional simulations, using an efficient local-orbital method. We focus on the PTB7-$PC_{71}BM$ blend which is commonly utilized for higher efficiency OSC's. We find low energy structural changes of the PTB7 donor can be reached by *local* motions of O or H atoms. PTB7 has an aromatic backbone connected to alkyl groups through bridging O atoms. In the first structural change the bridging O atom in the C-O-C configuration locally moves to form a C=O double bond with the aromatic chain. Two C-O single bonds are converted to a C=O double bond, leaving a dangling bond on the α-C atom and generating states within the electronic band gap. The defect energy is 2.17 eV, which may be reduced to ~1.61 eV in the

presence of excited electronic states. We estimate energy barriers of at most ~2.65 eV which are accessible with blue photons.

The second low-energy structural change involves the local motion of H from the β-C to the α-C of the alkyl chain, followed by a cleaving of the PTB7 polymer. A C-dangling bond forms on the β-C site accompanied by the generation of states within the electronic band gap. Here also two C-O single bonds in the C-O-C configuration, convert to a C=O double bond. The defect state has an energy of 2.22 eV which may be reduced to ~1.79 eV in the presence of excited electronic states. Both these local O and H motions provide lower energy pathways than the formation of CH_2 defects within the thiophene group. One defect annealing pathway is reversible back to the initial state. Surprisingly there are other pathways where the defects can anneal irreversibly to distortions of the PTB7 polymer. The irreversible changes are quite different from the reversible light-induced changes known for inorganic systems such as amorphous silicon.

The low-energy defects identified in our paper are dominated by the bridging O atom, which is a source of instability. We can infer that polymers such as P3HT, *without* the bridging O groups, may be more stable, and degrade at a slower rate. Such ab-initio approaches can provide a deep insight on light induced atomistic changes and physical insight on why certain organic materials are more stable than others. A future goal will be to design and identify organic materials, that can be more stable than present-day materials, and utilized in new generations of organic solar cells.

2.7 Methods

The local orbital based SIESTA method was used in computationally efficient calculations in a multi-processor environment. For the majority of PTB7 calculations 64 processors were used. To speed up the simulations we initially relax the structures with semi-empirical potentials using CHEMDRAW, and then use these coordinates as input to SIESTA.

2.8 Supporting Information

2.8.1. Measurement

Measurements of light induced degradation was carried out in an environmental chamber under a continuous flow of high purity N_2 gas, thereby avoiding exposure to moisture and oxygen during the entire course of the experiment. A xenon source solar similar with appropriate filters was used. Illumination was through a quartz window. The organic solar cells were illuminated through the glass substrate. Both the circulating N_2 gas and a fan inside the chamber were utilized to keep the sample near room temperature (~30 ºC). The environmental chamber had instrumentation to measure light current-voltage (I-V), dark I-V and defect densities in-situ, without exposing the sample to air. Intensity of the light was changed using a lens. Experimental measurements were carried out under constant exposure for 4 days (96 hours).

Fig. S1. Environmental chamber for measurement of light induced degradation of organic solar cell, showing two views.

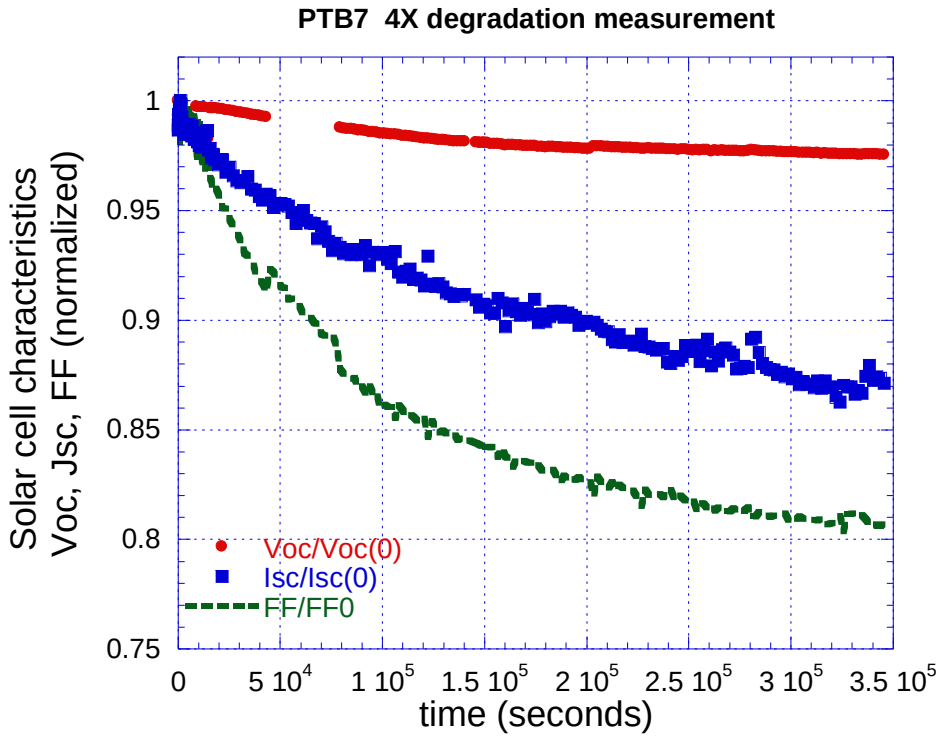

Fig. S2 Typical degradation [S1] of a PTB7-PCBM71 solar cell under light soaking of 4 suns in an environmental chamber with inert gas flow, for 96 hours, showing drops of open circuit voltage (Voc), short circuit current (Jsc) and fill factor FF. All values were normalized with respect to maximum value.

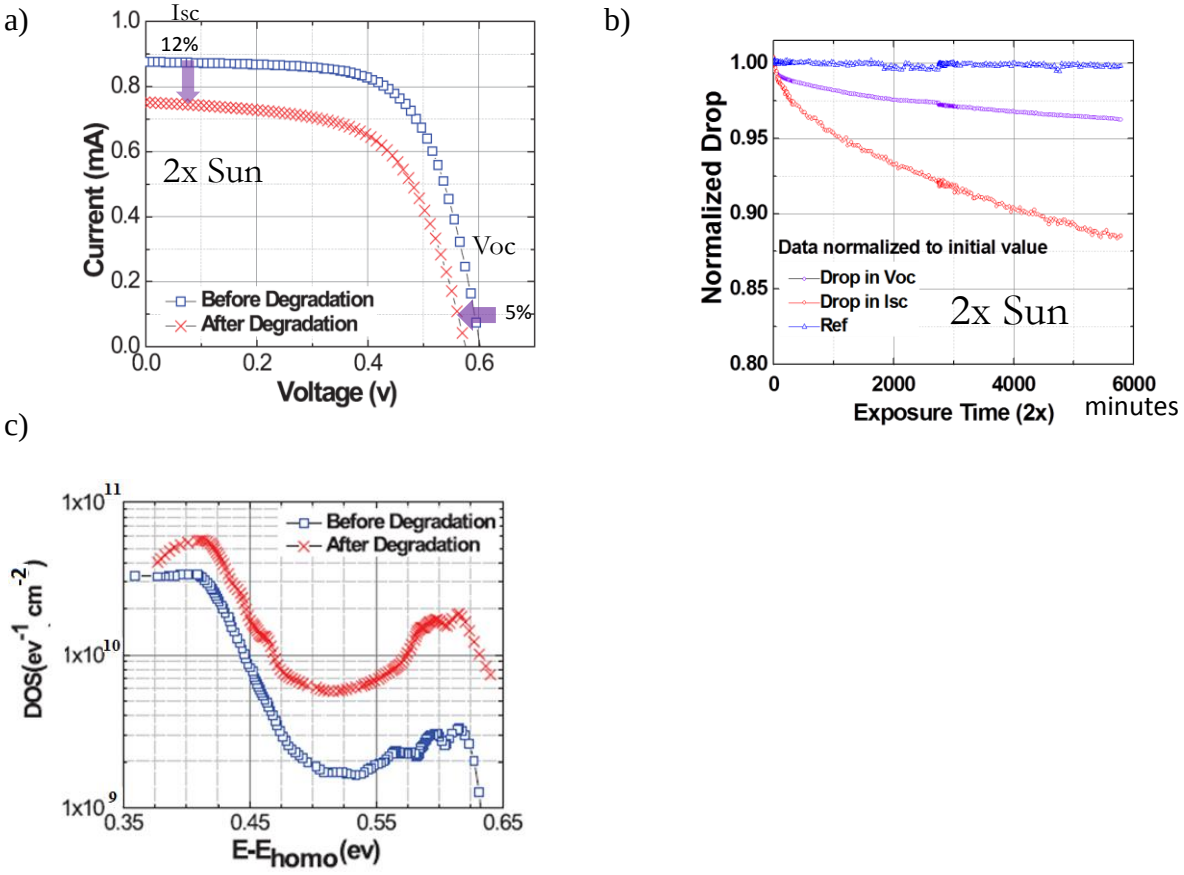

Fig. S3 Measured degradation of a P3HT PCBM solar cell for 96 hours under 2x illumination [S2] a) Current–voltage (I-V) characteristics before and after degradation. b) Normalized drops of Voc and Isc with light soaking time. c) Electronic densities of states measured relative to the HOMO level, before and after degradation.

References

[S1] P. Joshi, Ph.D. thesis Iowa State University (2016).

[S2] J. Bhattacharya, Ph. D. Thesis Iowa State University (2013).

2.9 Acknowledgements

We thank Prof. V. Dalal for simulating discussions. This research was partially supported by the National Science Foundation through grantCBET-1336134 (computational work); the Catron Foundation (computational work) and the Ames Laboratory, operated for the Department of Energy (theoretical analysis) by Iowa State University under contract No. DE-AC02-07CH11385. We acknowledge use of computational resources at the National Energy Research Scientific Computing Center (NERSC) which is supported by the Office of Science of the USDOE under Contract No. DE-AC02-05CH11231.

2.10 References

1. You, J.; Dou, L.; Yoshimura, K.; Kato, T.; Ohya, K.; Moriarty, T.; Emery, K.; Chen, C-C.; Gao, J.; Li, G.; et al A Polymer Tandem Solar Cell with 10.6% Power Conversion Efficiency. *Nat. Comm.***2013**, *4*, 1-10.

2. Liu, Y.; Chen, C.C.; Hong, Z.; Gao, J. ; Yang, Y. (M) ; Zhou, H.; Dou, L.; Li, G.; Yang, Y. Solution-processed Small-molecule Solar Cells: Breaking the 10% Power Conversion Efficiency, *Nature Scientific Reports***2013**, *3*, 3356-3361.

3. Park, S. H.; Roy, A.; Beaupre´, S.; Cho, S.; Coates, N.; Moon, J. S.; Moses, D.; Leclerc, M.; Lee, K.; Heeger, A. J. Bulk Heterojunction Solar Cells with Internal Quantum Efficiency Approaching 100%. *Nat. Photonics* **2009**, *3*, 297-303.

4. Dou, L.; You, J.; Yang, J.; Chen, C.-C.; He, Y.; Murase, S.; Moriarty, T.; Emery, K.; Li, G.; Yang, Y. Tandem Polymer Solar Cells Featuring a Spectrally Matched Low-bandgap Polymer. *Nat. Photonics***2012**, *6*, 180-185.

5. Jorgensen, M.; Norman, K.; F. Krebs, F.; Stability/Degradation of Polymer Solar Cells, *Solar Materials and Solar Cells***2008**, *92*, 686-714

6. Jorgensen, M.; Norman, K.; Gevorgyan, S.; Tromholt, T.; Andreasen, B.; Krebs, F.; Stability of Polymer Solar Cells, *Advanced Materials*, **2010**, *24*, 580-612.

7. Bhattacharya, J.; Mayer, R. W.; Samiee, M.; and Dalal, V. L., Photo-induced Changes in Fundamental Properties of Polymer Solar Cells, *Appl. Phys. Lett*. **2012**, *100*, 193501.

8. Street, R. A.; Krakaris, A.; and Cowan, S. R, Recombination through Different Types of Localized States in Organic Solar Cells, *Advanced Functional Materials*, **2012**, *22*, 4608-4619.

9. Street R. A.; and Davies, D. M.; Kinetics of Light Induced Defect Creation in Organic Solar Cells, *Appl. Phys. Lett*. **2013**, *102*, 043305.

10. Peters, C.H.; Sachs-Quintana, I.T.; Kastrop, J. P.; Beaupre, S.; Leclerc, M.; and McGehee, M. High Efficiency Polymer Solar Cells with Long Operating Lifetimes, *Adv. En. Mat*. **2011**, *1*, 491-494.

11. Street, R.; Northrup, J.; Krusor, B.J.; Radiation Induced Recombination Centers in Organic Solar Cells, *Phys. Rev. B.***2012**, *85*, 205211.

12. Northrup, J. Radiation Induced Hydrogen Rearrangement in Poly(3-alkylthiophene), *Applied Physics Express***2013,** *6*, 121601.

13. Staebler D. L.; Wronski, C. R. Reversible Conductivity Changes in Discharge-produced Amorphous Si, *Appl. Phys. Lett.***1977**, *31*, 292-294.

14. Lu, L.; Yu, L., Understanding Low Bandgap Polymer PTB7 and Optimizing Polymer Solar Cells Based on it, *Advanced Materials***2014**, *26*, 4413-4430

15. Sai, Na, Leung, K.; Za´dor J.; Henkelman, G. First Principles Study of Photo-oxidation Degradation Mechanisms in P3HT for Organic Solar Cells, *Phys. Chem. Chem. Phys.*, **2014**, *16*, 8092-8099

16. Soler, J. M.; Artacho, E. J.; Gale, D.; Garcia, A.; Junquera, J. ; Ordejon, P. ; Sanchez-Portal, D. The SIESTA Method for ab-initio Order_N Materials Simulation, *J. Phys. Condens. Matter***2002**, *14*, 2745-2779.

17. Troullier N. ; Martins, J. L.; Efficient Pseudopotentials for Plane-wave Calculations, *Phys. Rev.B***1991**, *43*, 1993-2006.

18. Perdew, J. P. ; Ernzerhof, M. ; Burke, K. Rationale for Mixing Exact Exchange with Density Functional Approximations *J. Chem. Phys*. **1996**, *105*, 9982-9985.

19. Endres, R.G.; Fong, C.Y. ; Yang, L.H.; Witte, G. ; and Ch. Woll,Ch,; Structural and Electronic Properties of Pentacene Molecule and Molecular Pentacene Solid, *Computational Materials Science***2004**, *29*, 362–370.

20. Liao, S-H. ; Jhuo H-Y.; Cheng, Yu-S.; Chen, S-An. Fullerene Derivative-Doped Zinc Oxide Nanofilm as the Cathode of Inverted Polymer Solar Cells with Low-Bandgap Polymer (PTB7-Th) for High Performance, *Advanced Materials*, **2013** , *25*, 4766–4771.

21. Bar-Yam, Y.; Joannopoulos, J. D. Silicon Self Interstitial Migration: Multiple Paths and Charge States, *Phys. Rev. B.* **1984**, *30*, 2216-2218.

22. Biswas,R.; Pan, B.C.; Ye, Y.; Metastability of Amorphous Silicon from Silicon Network Rebonding, *Phys. Rev. Lett*. **2002**, *88,* 205502.

23. Bhattacharya, J., Ph.D. thesis, Iowa State University (2013).

24. Stutzmann, M.; Jackson, W.; Tsai, C.C., Light Induced Metastable Defects in Hydrogenated Amorphous Silicon- a Systematic Study, *Phys. Rev. B***1985**, *32,* 23-42.

25. Branz, H., Hydrogen Collision Model; Quantitative Description of Metastability in Amorphous Silicon, *Phys. Rev. B***1999**, *59,* 5498-5512.

26. Burlingame,Q.; Tong, X.; Hankett, J.; Slootsky, M.; Chen, Z.; Forrest, S., Photochemical Origins of Burn-in Degradation in Small Molecular Weight Organic Photovoltaic Cells, *Energy Env. Sci.* **2015**, *8,* 1005-1010.

27. Wong H.C., Li, Z.; Tan, C.H.; H. Zhong, H.; Huang, Z.; Bronstein, H.; McCulloch, I.; Cabral, J.T.; Durrant, J.R., Morphological Stability and Performance of PolymerFullerene Solar Cells under Thermal Stress: The Impact of Photoinduced PC60BM Oligomerization, *ACS Nano***2014**, *8,* 1297-1308.

28. Guerrero, A. ,Heidari, H. ; Ripolles, T. S. ; Kovalenko, A. ; Pfannmöller, M.; Bals, S.; Kauffmann, L-D.; Bisquert, J.; and Garcia-Belmonte, G., *Adv. En. Mat.***2015**, 5, 1401997.

CHAPTER 3. UNUSUAL INFRARED ABSORPTION INCREASES IN PHOTO-DEGRADED ORGANIC FILMS†

Satvik Shah[a,b] *, Rana Biswas*[*a,b,c]*, , Thomas Koschny*[a]*, Vikram Dalal*[a,b]

Adapted from a paper published in Nanoscale 9, 8665-8673 (2017)

3.1 Abstract

Degradation is among the most pressing problems facing organic materials, occurring through ingress of moisture and oxygen, and light exposure. We determine the nanoscale pathways underlying degradation by light-soaking organic films in an environmental chamber, and performing infrared spectroscopy, to identify atomic bonding changes. We utilize as a prototype the low band gap PTB7-PCBM blend. Films light-soaked in the presence of oxygen show unusual increased absorption at 1727 cm^{-1} attributable to increased C=O modes, and a broad increase at 3240 cm^{-1} attributable to hydroxyl (O-H) groups bonded within the organic matrix. Films exposed to oxygen in the dark, or light-soaked in an inert at-mosphere, do not exhibit significant absorption changes, suggesting simultaneous exposure of oxygen and light that creates singlet excited oxygen is the detrimental factor. Our ab-initio electronic structure simulations interpret these by oxidation at the α-C site of the alkyl chains in PTB7, with an irreversible rupture of the alkyl chain and formation of new C=O and C-O-H conformations at the α-C. Infrared spectroscopy coupled with ab-initio simulation can provide a powerful tool for quantifying photo-structural atomic bonding changes. Understanding nanoscale light-

induced structural changes will open avenues to designing more stable organic materials for organic electronics.

3.2 Introduction

Organic electronics are a very appealing platform for low cost, flexible solar cells and displays. A primary problem in organic materials is their stability. One of the primary roadblocks preventing commercial deployment of organic photovoltaics (OPVs) is their instability during light exposure, often in a few hours or days[1,2,3]. Such stability issues are also a major concern in the new perovskite family of solar cells[4,5].

The photo-degradation of OPVs in the presence of light and ultraviolet (UV) exposure[1,6-12] show the loss of short circuit current (J_{sc}), open circuit voltage (V_{oc}), fill factor (FF), and efficiency after light-soaking in inert and ambient environments. Measurements of mid-gap states in films found increases in mid-gap densities of electronic states with light and UV exposure, with a hint of stabilization at long time[6]. It is well-recognized that energetic blue and UV photons can break bonds and lead to structural changes in organic materials. The oxidation of conjugated vinylene groups has been char-acterized[1,2] and detailed measurements have identified the diffusion of metal from the cathode, and In from the ITO

Organic electronics are a very appealing platform for low cost, flexible solar cells and displays. A primary problem in organic materials is their stability. One of the primary roadblocks preventing commercial deployment of organic photovoltaics (OPVs) is their instability during light exposure, often in a few hours or days1,2,3. Such stability issues are also a major concern in the new perovskite family of solar cells4,5.

The photo-degradation of OPVs in the presence of light and ultraviolet (UV) exposure1,6-12 show the loss of short circuit current (Jsc), open circuit voltage (Voc), fill

factor (FF), and efficiency after light-soaking in inert and ambient environments. Measurements of mid-gap states in films found increases in mid-gap densities of electronic states with light and UV exposure, with a hint of stabilization at long time6. It is well-recognized that energetic blue and UV photons can break bonds and lead to structural changes in organic materials. The oxidation of conjugated vinylene groups has been char-acterized1,2 and detailed measurements have identified the diffusion of metal from the cathode, and In from the ITOcontact, as potential sources of degradation. Hole-transport layers such as PEDOT:PSS and the various interfaces in organic solar cells (OSCs) have been suggested to cause instability.[1,2] The widely studied prototypical polymer organic solar cell (OSC) with 3-4% efficiency, comprises P3HT–PC60BM, with alkyl chains attached to the thiophene group (Fig. 1a). These solar cells exhibited creation of mid-gap states in ~96 hours of light-exposure in an environmental chamber under nitrogen flow[8]. Street et al[13] observed a near stabilization of the defect density over several days for PCDTBT:PC70BM cells. Much longer light exposure (exceeding a year), observed an initial burn-in period where OSC characteristics drop nearly exponentially, followed by a slow linear decay.[7,14] The low band gap polymer PCDTBT (utilized for higher efficiency (>6%) solar cells), have alkyl chains bonded to N in the aromatic backbone (Fig. 1b) may exhibit higher stability than P3HT-PCBM.[15] OSC stability also depend on the conformation of the polymer, as illustrated by the low band gap polymer PTB7, used in higher efficiency (7-9%) solar cells (Fig. 1c), which has alkyl chains connected to an aromatic backbone via a bridging O atom. PTB7 shows lower stability[16] and faster light-induced degradation than the P3HT based solar cells, with recent studies indicating the fill factor and short circuit current degrade the most.[17]

These observations suggest that the atomic configuration of the polymer strongly influences photo-induced changes and photo-stability. Utilizing rigorous ab-initio simulations, Northrup[18] and Street et al[13], proposed that local H-motion from the α-C to the thiophene ring forming a CH_2 defect could account for many features of the P3HT and P3AT (A= alkyl)photo-degradation. Electron paramagnetic resonance after light-irradiation of polymer (PBDTTT)-fullerene blends recently established metastable C-dangling bonds as the spin-active defect19 and it is of great interest to identify the chemical bonding changes generating such spin-active defects. Experiments on oxidized PTB7 and PTB7:PC70BM blends observed changes in the Raman spectrum, attributed to oxidation within the benzo-dithiophene (BDT) portion of the aromatic backbone.[16] The formation of singlet oxygen, from non-geminate triplet excitons, has also been proposed to cause instability.[20] In our previous work[21] we simulated intrinsic defect formation from reconfiguration of PTB7 occurring through local O and local H-motion. In spite of these intriguing proposals, there have been just a few studies16 on experimentally characterizing the structural changes during the degradation process, and correlating the changes with ab-initio calculations. There has been relatively little fundamental understanding of what organic polymer atomic conformation, can lead to more stable devices, and how organic materials may be designed to be more stable.

To avert the complexity with interfaces, electron-transport and hole-transport layers in OSCs, we focus on the stability of the intrinsic absorber layer alone here. Changes in device architecture (e.g. using an inverted OSC) cannot avert the instability underlying the absorber layer. This has led us here, to experimentally characterize through infrared (IR) spectroscopy, structural changes in the organic polymer films on standard salt substrates, induced by light-soaking. We focus on the low-band gap donor-acceptor PTB7-PCBM blend, since this has led

to higher efficiency solar cells (η~7-9%).17 We find large measurable changes in infrared absorption before and after light-soaking in the presence of oxygen. We interpret the results with our ab-initio calculations of light-induced bonding rearrangements.

Our approach is to spin coat organic polymer absorber layers on infrared (IR) transparent salt (NaCl) substrates, under the same conditions and thicknesses in OSCs. For donor-acceptor blends we expect the same bulk morphology in films that were present in devices. As-deposited (pristine) films, isolated from moisture and oxygen, were characterized with IR spectroscopy, to identify IR-active vibrational modes. The organic films were then light-soaked in an environmental chamber, under inert N_2, ambient air and dry air conditions, and their infrared absorption was re-measured. The light-soaked films were compared with the reference pristine film, to identify atomic bonding changes. Interpretations of atomic bonding changes and IR absorption changes, can be made more readily for films than in complex solar cell structure where multiple layers and interfaces can contribute. Moreover infrared spectroscopy is a powerful tool since the polymers have strong infrared-active modes, dominated by CHn (n=2 being the dominant species, and n=3 much weaker) in the alkyl chains (Fig. 1), C-S in the thiophene groups, C-O or C-F in PTB7-PCBM, and bending vibrations in the aromatic backbone. Significant changes in the infrared absorption spectrum indicate that a sufficient density of species show conformational changes, and our work may be among the first to find such measureable changes in infrared spectra.

3.3 Experimental

The organic films were spin-coated on salt (NaCl) substrates, since NaCl is transparent to IR from 4000 cm-1 to 650 cm-1 as confirmed by its featureless IR absorption. A solution of PTB7 polymer (1-Material, 10 mg) and PC60BM (Nano-C, 15 mg) in dichlorobenzene solvent

(Sigma Aldrich, 0.97 mL) and 1,8-Diiodooctane (DIO) additive (Sigma Aldrich, 0.03 mL (i.e. 3%)) was prepared in the glove-box and stirred for 12 hours at 75 °C and 300 rpm. The PTB7:PC60BM blend was spin-coated on the NaCl salt substrate at 600 rpm for 60 seconds, in the glove-box. The sample was then dried at 100 °C for 30 minutes on a hot-plate. For these deposition conditions the film

(a)

(b)

(c)

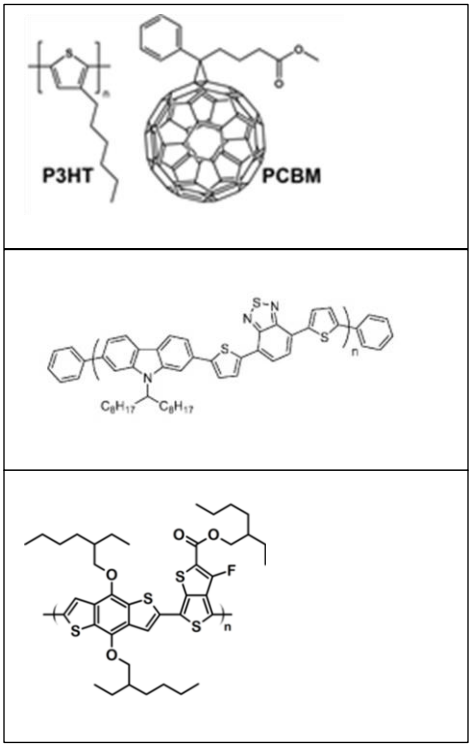

Fig. 1 Molecular structures of a) P3HT-PCBM, b) PCDTBT, and c) PTB7

thickness was ~100 nm, typical of the absorber layer in PTB7: PC60BM OSCs.

Previous experiments on PTB7-PCBM by Guo et al 22 found that annealing at 120 °C for 30 minutes did not change optical properties but significantly reduced the short circuit current and power conversion efficiency of the organic solar cell. We did not anneal at such higher temperatures (120 °C) which can alter the lamellar packing of the PTB7, but took care to dry our films at 100 °C. We consider drying as an important step to remove the solvent and

the additive from our spin-coated films which can introduce unwanted features in the infrared absorption spectrum. We compared PTB7:PC60BM films that were annealed at 100 °C for 10 min and 30 min, and found the IR absorption of these to be very similar (supplementary Fig. S1). This indicated that that IR absorption was insensitive to the anneal time.

Spin-coating and drying processes were performed in the nitrogen filled glove-box, where H2O and O2 levels were only a few ppm. To perform the light-induced degradation, illumination of the samples was carried out in an environmental chamber (Fig. S2, ESI) at 4X Sun intensity for 24 hours, under conditions of (i) inert N_2 flow, (ii) ambient air atmosphere containing both oxygen and moisture, and (iii) dry air consisting of 70:30 N2:O2. The circulating gas and a fan inside the chamber were utilized to keep the sample near room temperature (~30 ºC).

Pristine (un-degraded) and light degraded samples were sealed in an air-tight transfer-tube for Fourier-Transform IR (FTIR) spectroscopy. FTIR spectroscopy was performed in a Bruker Vertex 70V FTIR spectrometer. The samples on NaCl substrates were placed within the sample chamber in vacuum to avoid exposure to the atmosphere. Infrared transmission measurements were performed for two reference configurations comprising of i) no sample – straight transmission ii) NaCl substrate (without) organic film. Transmission measurements of pristine and light-degraded films were performed at room temperature, over ~2 hours, allowing the measurements to stabilize. Transmission measurements were performed with the beam incident on the uncoated surface of NaCl, although the transmission through the coated surface is equivalent, due to reciprocity. To identify absorption changes, we referred both the pristine and light-degraded films to the bare NaCl substrate as the reference.

3.4 Results and discussion

PTB7 is an intra-molecular donor-acceptor configuration with thienothiophene (TT) and benzodithiophene (BDT) pairs, forming the hole transport phase in OSCs. The donor TT units contain electronegative F, whereas the acceptor BDT has two thiophene groups (Fig. 1c). PCBM is the commonly used acceptor and electron transport phase.

IR spectroscopy has a sensitivity of a few parts in 1000, and is not expected to measure changes below such a threshold. It is known6,8 that the OSC density of electronic states changes after light soaking in N_2 are in the range of 10^{17} cm^{-3}, or 1 atom in 10^5 and such changes are not expected to be resolved in IR measurements. IR measurements probe much larger changes in atomic bonding configuration.

We performed IR spectroscopy of pristine and light-soaked PTB7:PCBM films, that were light-soaked in N_2, ambient air and dry air (in a mixture of 70:30 N2:O2). Additionally, we kept films in the dark in an ambient atmosphere for one week and re-measured their IR absorption. The largest measurable changes in the IR absorption were observed in films that were light-soaked in dry air or in the ambient atmosphere. No measurable changes were observed for films exposed to air in the dark, implying that oxygen or moisture alone does not cause degradation. Instead it is necessary to have a combination of oxygen and light. The likely interpretation is that light excites triplet molecular oxygen to its excited singlet state (O_2*), which in turn reacts with organic species.

We measured the infrared transmission of pristine PTB7:PC60BM blend (Fig. 2a, b) and the light-degraded blend (Fig. 2) films in N_2, utilizing the reference of a bare NaCl substrate. For clarity of interpretation, we divide the IR absorption spectrum into i) the higher frequency region above 2000 cm-1 (Fig. 2a) and ii) the lower frequency region between 1000-

2000 cm-1 (Fig. 2b). Standard infrared absorption tables23,24 are utilized to identify the inter-molecular species contributing to the vibrational modes. Among the principal IR-active species contributing to the absorption, are the large density of ethyl (CH2) groups within the alkyl chains, that are connected to the aromatic backbone. The well-known six vibration modes of the CH_2 group with their gas phase vibrational frequencies, consist of the asymmetric stretch (~2926 cm^{-1}), symmetric stretch (~2853 cm^{-1}), scissor bend (~1450 cm^{-1}), twist (~1250 cm^{-1}), in-plane wag (~1250 cm^{-1}), and a low frequency rocking mode (~720 cm^{-1}). Such CH2 modes are found in our measurement, albeit at slightly shifted frequencies.

The pristine PTB7-PCBM film (Fig. 2a) displays well-defined IR-active vibrational modes, that we index (Table 1), utilizing the standard IR assignments[23,24] to be: 1) A closely spaced doublet at 2961 and 2933 cm^{-1} assigned to the asymmetric CH2 stretch vibration. 2) A weaker absorption feature at 2867 cm^{-1}, assigned to the CH2 symmetric stretch. 3 and 4) Below 2000 cm^{-1} there are a rich variety of modes for pristine PTB7 (Fig. 2b) arising from bending and stretching vibrations. A mode pair at 1728 cm-1 and 1705 cm-1 can be assigned to stretch modes of C=O in the O-C=O configuration in PTB7, corresponding to the ester conformational geometries (RO-C=O; R=alkyl). PCBM also contributes to C=O stretching modes. 5) The 1569 cm-1 mode is ascribed to the IR-active combination of C=C stretch in the TT and BDT units in the aromatic backbone that have a weak infrared active absorption. In Raman measurements16 these produce weak Raman active modes at 1549 cm-1 and 1578 cm-1. 6) The weak shoulder at 1458 cm-1 can be assigned to the methyl (CH3) asymmetric bend, since CH3 conformations cap the alkyl chains. CH3 capping groups are far fewer that CH2, resulting in much weaker CH3 features. 7) The strong 1431 cm-1 absorption can be assigned to the CH2 scissor bend. 8) The weak feature at ~1400 cm-1 is assigned to the CF stretch, from the single

F atom within the conjugated portion of PTB7. 9) A weak 1367 cm-1 feature assigned to the CH3 symmetric bend, is paired with its symmetric bend (see 6) at 1458 cm-1. 10 and 11) The two overlapping modes at 1294 cm-1 and 1261 cm-1, can be assigned to a combination of the asymmetric C-O-C stretch and the CH2 twist, which both lie in this region. 12) The 1183 cm-1 feature is assigned to a C-O stretch in the ester functional group, present in the TT portion of PTB7, containing the ester conformation R-O-C=O (COOR). 13) The 1153 cm-1 mode is assigned to the CH2 in-plane wag. 14) The 1061 cm-1 mode likely arises from the C-O-C symmetric stretch, a counterpart of its asymmetric stretch (10) at 1294 cm-1.

We performed a photo-degradation of the PTB7:PCBM blend film in an inert N2 atmosphere in an environmental chamber. All of the IR absorption features of the pristine are also found in the degraded PTB7 sample (Fig. 2; Table 1), albeit with slightly shifted wavelengths (by ~2-3 cm-1), but with similar line shape. The high frequency region (4000 cm-1 to 2000 cm-1, Fig. 2a) depict similar features for the pristine and N_2 photo-degraded blend except for some change in the overall slope. We performed the photo-degradation of PTB7-BCBM blend films in ambient air (in the presence of oxygen and moisture, with a relative humidity ~40-50%) instead of the inert N2, (Fig. 3a, 3b), similar to the measurements of Razzel-Hollis et al.[16] We observe much larger changes in the IR spectrum of the light-degraded blend in the ambient atmosphere. The features of the ambient degraded film are much weaker than the pristine film and the smaller absorption features of the pristine film are not apparent. We find a stronger absorption feature at 1727 cm-1 and a new broad and weak absorption mode at 3240 cm^{-1} appearing in the ambient-degraded blend film (Fig. 3). The strong 1727 cm^{-1} feature arises from C=O bond stretching modes. Although C=O bonds are present in the pristine film, this feature has much higher strength in the ambient-degraded blend film,

Table 1. Absorption features in the PTB7-PCBM blend in the pristine state, after light soaking in an inert N_2 atmosphere, in ambient atmosphere, and dry air

	pristine	Light degraded in N_2	Light degraded in ambient	Light degraded in dry air
Mode	Peak (cm^{-1})	Peak (cm^{-1})	Peak (cm^{-1})	Peak (cm^{-1})
O-H stretch	--		3240	(weak) 3200
CH_2 asymm. stretch	2961	2961		2960
CH_2 asymm. stretch	2933	2933	2911	2911
CH_2 symm. stretch	2867	2867	2844	2878
C=O str. (aldehyde)	1728	1728	1727	1727
C=O str. (ester)	1705	1705	1719	
C=C aromatic str.	1569	1569	1600	1600
CH_3 asymm. bend	1461	1461		1458
CH_2 scissor bend	1431	1431	1425	1431
CF stretch	1400	1400		
CH_3 symm. bend	1367	1367		
Asymm. C-O-C stretch + CH_2 twist	1294	1294		
Asymm. C-O-C str; + CH_2 twist	1261	1261	1222	
C-O stretch (ester)	1183	1183		
CH_2 wag	1153	1153		1153
C-O-C symm. stretch	1061	1061	1058	1053

suggesting an increase of C=O bonds when photo-degradation is performed in oxygen environments. At the wavelength of 1600 cm^{-1} there is a significant increased absorption in dry air, and a weak absorption in ambient- a feature that was absent in the pristine blend. The weak 3240 cm^{-1} feature can be ascribed to stretching modes of O-H bonds from bonded H in the structure in a C-O-H configuration. This is distinguished from molecular water absorption modes that occur above 3600 cm-1 which may also be slightly present. Very few bond-stretching conformations produce vibrational modes at such high frequencies. Trapped water (H_2O) has significantly higher frequency modes, between 3600 cm^{-1} and 3800 cm^{-1}, and cannot contribute to the 3240 cm^{-1} feature. An alternative candidate is the N-H vibrational modes

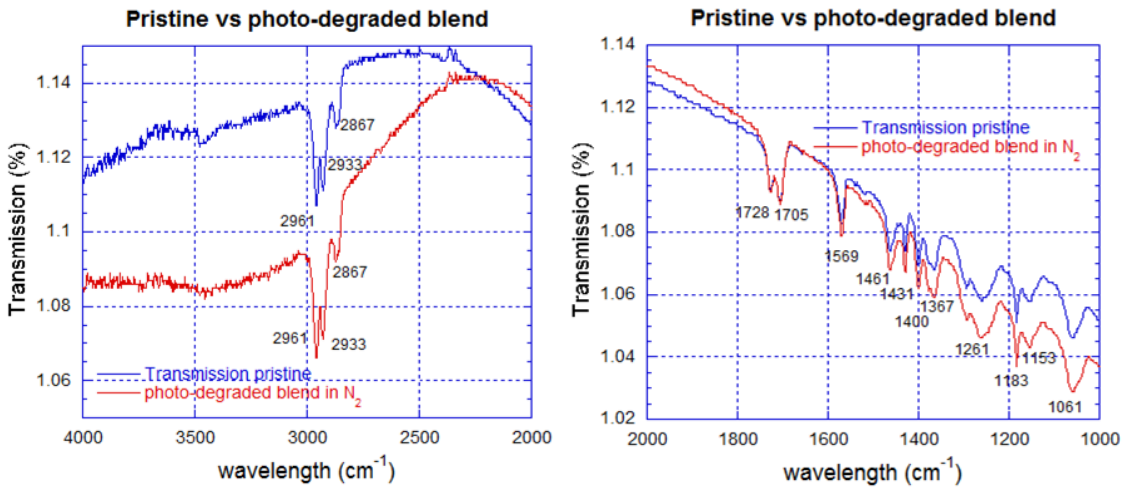

(a) (b)

Fig. 2. Measured infrared (IR) transmission spectra of PTB7:PCBM blend film. Pristine film and photo-degraded in N_2 film at a) high frequency (4000 cm-1 to 2000 cm-1), and b) at low frequency (2000 cm^{-1} to 1000 cm^{-1})

which occur in this region. However, there are no N sites in PTB7 and we can rule out the presence of N-H or trapped ammonia species in the sample.

To assess the relative importance of moisture and oxygen, we performed light soaking in dry air (with a 70:30 N_2:O_2 mixture) (Fig. 3c, d). We observed increased absorption of the 1727 cm-1 mode from C=O bonds (Fig. 3d), a similar photo-degradation feature seen in ambient air. There is also a broad weak absorption at 3200 cm-1 (Fig. 3c) suggesting also O-H bonds from bonded H in the structure in a C-O-H configuration. Since the results of photo-degradation in ambient air and dry air are very similar, we infer that moisture has negligible effect, and the primary source of degradation is oxygen in the presence of illumination. Furthermore, photo-degradation in N_2 does not cause significant changes in absorption spectra, strengthening our conclusion that O_2 with light is the primary degradation source. We also kept the pristine blend films in the dark under ambient conditions (in the presence of oxygen and moisture). However,

no significant changes in the absorption spectra were found. This suggests that illumination combined with oxygen is necessary to cause degradation.

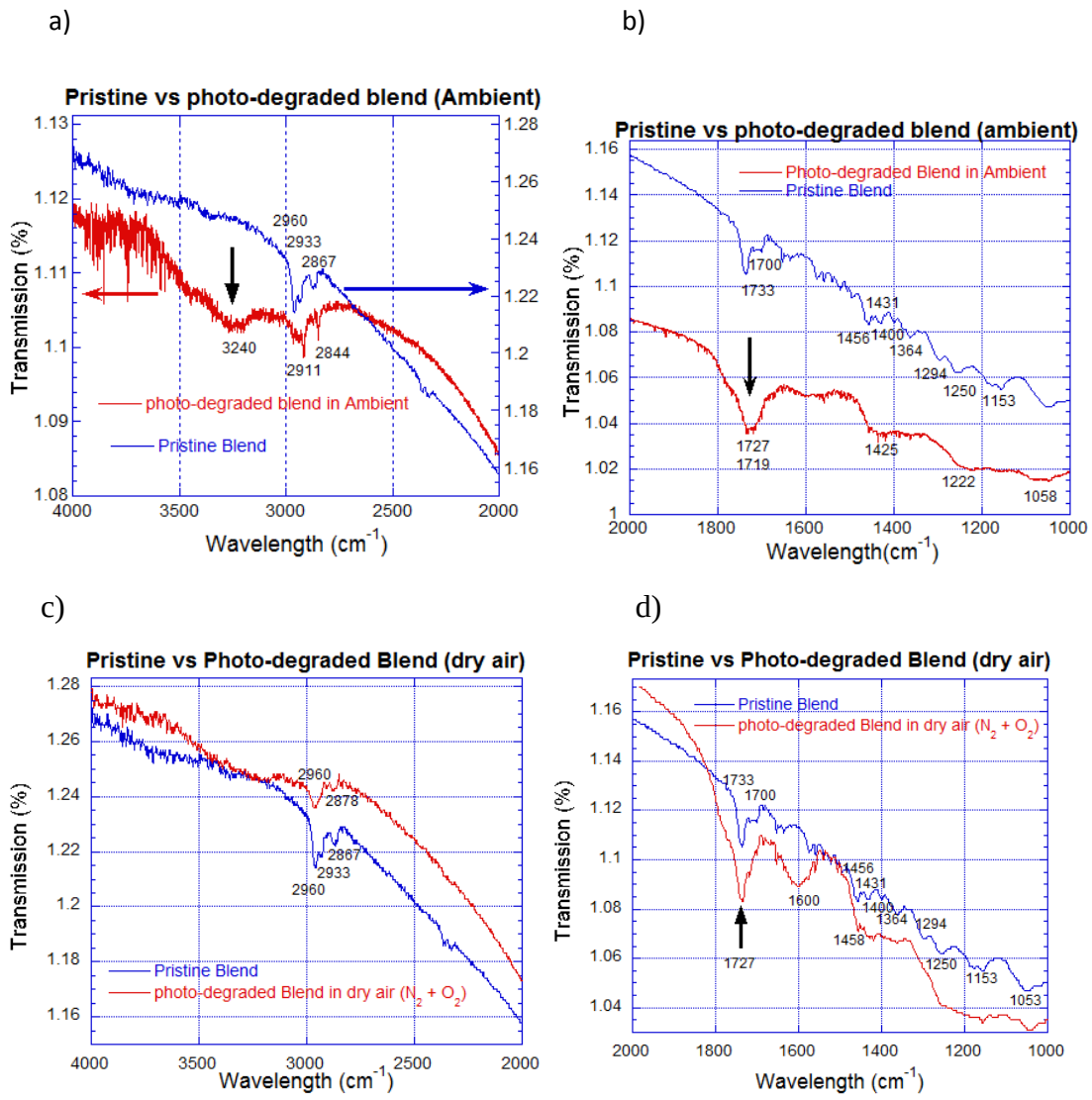

Fig. 3 Measured infrared (IR) transmission spectra of PTB7:PCBM blend films. Pristine and photo-degraded in ambient air atmosphere blend film at a) high frequency and b) at low frequency. Pristine and photo-degraded in dry air (N2:O2 70:30) at c) high frequency, and d) at low frequency.

The most significant change occurs when the PTB7:$PC_{60}BM$ blend is light-soaked under ambient atmospheric conditions or in dry air. The appearance of strong absorption at 1727 cm-1 (Fig. 2b, 2d) corresponds to a strong C=O stretch vibration mode. This is

accompanied by new broad absorption at 3240 cm-1 attributable to O-H stretch for hydroxyl groups bonded within the organic matrix. The likely source of these features is the oxidation of the PTB7, in which the O_2 molecule is photo-excited from its triplet ground state to the excited singlet state (O_2*). O_2* is well-known to be very reactive and can oxidize organic molecules with vinylene groups (e.g. MEH-PPV) to form C-O-O-C ring conformations or C=O conformations.1 Our simulations below suggest O_2* can attack PTB7 at the αC site, well-known to be the most reactive C site. PTB7-PCBM films left in the ambient atmosphere in the dark over several days do not show significant absorption changes, in spite of continuous exposure to oxygen and moisture. This is consistent with triplet O2 being unreactive and the role of light exposure to excite triplet O_2 to singlet O_2* as the initiating step to degradation.

3.5 Ab-initio simulations

We performed ab-initio simulations to identify a pathway for oxidation of PTB7. The Spanish Initiative for Electronic Simulations with Thousands of Atoms (SIESTA)25 method was employed to simulate the electronic properties. Ab-initio density functional theory (DFT) with the SIESTA method utilized Troullier-Martins norm-conserving pseudo-potentials26, in a fully non-local form, with a basis set of multiple-zeta pseudo atomic orbitals. The self-consistent potential was calculated on a real space grid whose spacing was determined by an energy cut-off of 100 Ry. We used the general gradient approximation (GGA) using the Perdew-Burke-Ernzerhof (PBE) parametrization of the exchange-correlation functional27 to treat the nonlocal exchange and correlation energies. We obtain the electronic structure, density of states, and total energies. The local-orbital based SIESTA method allows computationally efficient calculations in a multi-processor environment. Structural relaxation is performed with a steepest descent algorithm to obtain low energy configurations. Although

PTB7 is a polymer we adopted a 105-atom segment of the PTB7 chain by capping the ends of the conjugated segment with H atoms. This permitted the use of a simulation cell (with 2.41 nm x 2.15 nm x 1.35 nm dimensions) with periodic boundary conditions. We started with the fully relaxed PTB7 (Fig. S4, ESI) as the reference configuration, that does not have any levels within the electronic band gap, and a HOMO-LUMO separation of 1.54 eV, slightly smaller than the experimental band gap of 1.63 eV. We simulate external O_2 reaction with the α–C, and find the αC loses an H, which transfers to the neighbouring β-C (Fig. 4). The oxygen molecule bonds to the αC resulting in the O=C-O-H configuration, with a new C=O bond and a new C-O-H group at the αC (Fig. 4b). The bridging Cα-O-C between the polymer and the aromatic backbone remains undisturbed. Schematically this reaction is represented as

$$O_2{}^* + (\ldots\text{-O-}CH_2\text{-}CH_2\ \ldots)\text{alkyl}\ \ (\ldots\text{-O-COOH..})\text{alkyl} + [\text{--}CH_3]\text{alkyl}\quad (1)$$

The simulated enthalpy change for this reaction was -5.76 eV. The large energy gain is expected since the initial O-O (bond energy 5.15 eV), C-C (3.6 eV), and two C-H (4.4 eV-ethyl) are converted to C-H (4.57 eV- methyl), C=O (7.7 eV), C-O (3.71 eV), and O-H (4.81 eV). A net energy gain ~3.24 eV (i.e. 20.79 -17.55 eV) is estimated. The new C=O configuration at the αC, results in the increased absorption at 1727 cm^{-1}, observed in degradation with ambient or dry air. There is a new hydroxyl group at the αC, belonging to a carboxylic acid (COOH) configuration, and this OH stretch is expected to generate broad IR absorption modes in the high frequency region (3100-3400 cm^{-1}). We do observe a new weak IR absorption at 3240 cm^{-1} in ambient or dry air degraded blend films (Fig. 3), that corresponds to this hydroxyl stretch mode at α-C. The stretch frequency is significantly lower than that of OH in water molecules (>3600 cm^{-1}).

The alkyl chain ruptures and breaks away from the α–C site. After the oxidation reaction, the alkyl chain is capped by the βC with a methyl CH3 group (Fig. 4b). The oxidation is an irreversible degradation pathway in which the polymer chain detaches from the aromatic backbone. Since the αC remains bonded to the aromatic backbone through a C-O-C bridge (Fig. 4b) the symmetric and asymmetric C-O-C vibrational modes are largely unchanged, consistent with the observed IR absorption (Fig. 3).

We envisage an alternative oxidation pathway can involve C=O formation on the α-C and a C-O-H on the α-C, leaving two C-H bonds on both α-C and α-C, represented by:

$O2^{*}$+ (…-O-CH_2-CH_2 …)alkyl (…-O-COH..)alkyl + [--O=CH]alkyl (2)

Such a reaction would also be consistent with the observed increases of C=O and C-O-H bonds, and the rupture of the PTB7 monomer.

3.6Auxillary absorption changes

In addition to the significant changes to the IR absorption at 3240 cm-1 and 1727 cm-1, there are additional IR changes after photo-degradation. A notable change is the increased absorption at 1600 cm-1 after degradation in dry air (Fig. 3(d)) that also appears as a weak feature for the degradation in ambient (Fig. 3(b)). Although water has H-O-H bending modes near 1600 cm^{-1}, our observed absorption increase at 1600 cm^{-1} cannot be simply interpreted as due to water since the change occurs in dry air in the absence of moisture, and is not accompanied by significant increases in the O-H stretch at 3500-3600 cm^{-1}.

We suggest that the increased absorption at 1600 cm^{-1} maybe linked to changes in the aromatic backbone. In previous ab-initio simulations of PTB721 we observed the local motion

of the bridging O to the aromatic backbone to form C=O, and leaving behind a C-dangling bond on the α-C (Fig. 5). Our simulations indicate the local reconfiguration has an energy

(a) (b)

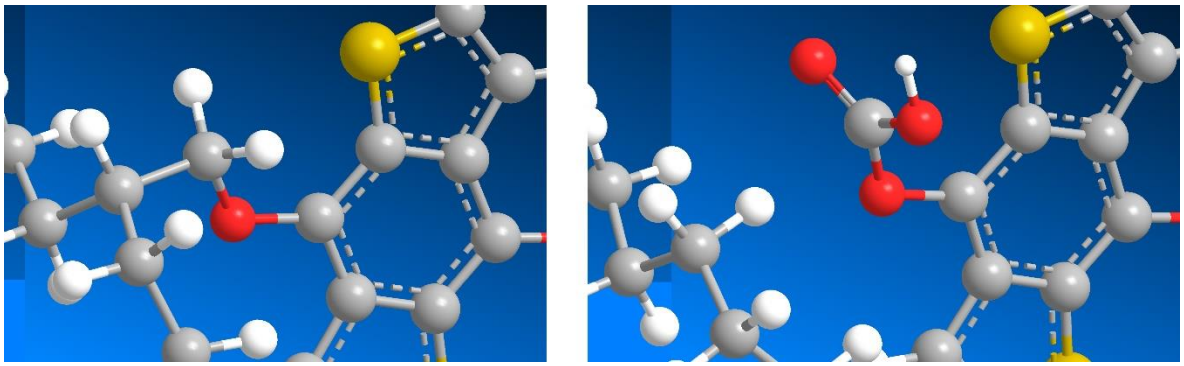

Fig. 4. Ab-initio simulations of the oxidation of the PTB7 polymer. a) The starting configuration showing a portion of the PTB7 monomer (Fig. S4, ESI) in which the bridging O is bonded to αC and the aromatic backbone. b) The degraded configuration with C=O and C-O-H formation at α–C, resulting in the irreversible cleavage of the polymer.

barrier near 2.7 eV which can be surmounted with blue photons, with a net change in enthalpy of 2.17 eV. This internal re-configuration causes a loss of aromaticity in the backbone, and two C=C and four C-C in-ring bonds (Fig. 5b), forming a cyclic alkene configuration. The C=C stretch modes for cyclic alkenes are known to occur between 1566-1650 cm-1 [23]. and can explain the increased 1600 cm-1 absorption. This internal reconfiguration also increases the C=O stretch at 1727 cm^{-1}, but would not affect high frequency modes near 3200 cm^{-1}.

External O_2 or O_2* is not directly needed for this reconfiguration, but our experiments suggest that light soaking in O-containing dry air can be effective in driving this reaction, although light soaking in the presence of moisture is less effective. More studies are needed to quantify these changes.

Photo-degradation in either ambient or dry air (Fig. 3(b), 3(d)) shows i) an overall decrease of the absorption (especially at lower frequencies) and ii) the absence of fine absorption features seen in the pristine sample.

We investigated the role of the NaCl substrate by photo-exposure of the bare uncoated NaCl in ambient atmosphere (Fig. S6 ESI). No new IR absorption features were induced in the NaCl substrate on light exposure. There is an overall decrease in NaCl substrate transmission by ~8% after photo-degradation in ambient atmosphere and 0-10% in dry air depending on the wavelength, (Fig. S6). This agrees with the observed reduction of transmission for the PTB7-PCBM blend samples after degradation (Fig. 3(a,b)). The 0.5 cm thick NaCl disks show some white

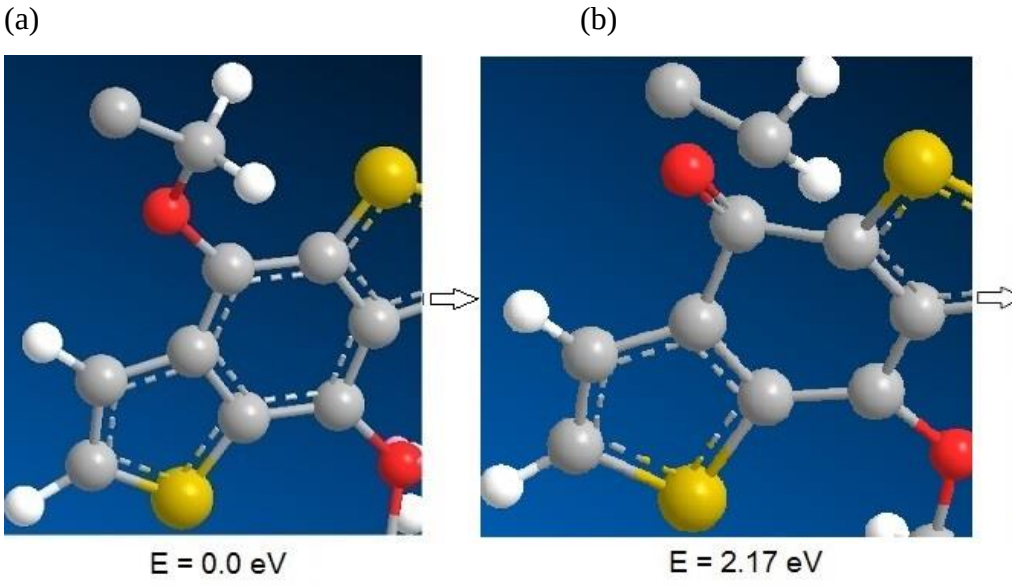

Fig. 5. Ab-initio simulations of O motion from a) the O bridging configuration between □C and the aromatic backbone to b) a C=O bond in the backbone, resulting in a cyclic alkene configuration with C=C and C-C bonds. A dangling bond appears on α-C.

discoloration after photo-degradation in ambient air, that causes scattering of the incident IR radiation. Since the NaCl is polycrystalline, it is likely that photoexposure develops finer scale polycrystalline grains in the NaCl that causes scattering. This scattering can dampen fine IR features observed in the pristine blend film. A magnified view of Fig. 3(b,d) reveals that the fine IR absorption features (between 1000-2000 cm^{-1}) in the pristine film (Fig. 3) are present but far weaker in the photo-degraded film, and more difficult to distinguish from the background.

3.7 Pathways for nanoscale bond conformation

The previously suggested local H-motion from the α-C to the thiophene creating a CH_2 defect within the thiophene group13,18 would leave the bridging oxygen C-O-C configuration unchanged, and would not be able to generate new C=O or C-O-H configurations. In previous simulations21 we found intrinsic defect formation from reconfiguration of PTB7 (without external O_2) by i) local motion of the bridging O to the thiophene forming sequentially C=O and then C-O-H (but no C=O), and ii) local H motion21 from the α-C to the β-C, producing a shifted C-O-C bridge. However additional C=O and C-O-H were not simultaneously produced in these pathways.

Raman spectroscopy16 suggested oxidation of PTB7 can form hydroxyl bonds on two equivalent CH sites within the TT unit at the 3,5 positions in the thiophene group, which however does not increase C=O bonds. A suggested pathway to stabilize PTB7 is replacement of H at these sites by fluorine, since the hydroxyl formation would be eliminated. Fluorine substitution to synthesize PTBF2 and PTBF3 has been achieved.28 Fully fluorinated PTBF3 exhibits better photo-stability27 since the F prevents O-H bond formation within the aromatic backbone. However the fluorinated analogs PTBF2 and PTBF3 exhibited lower efficiencies of 3.2% and 2.3-2.7% respectively, markedly lower than the 7-8% of standard PTB7 (i.e. PTBF1), since the band gap widened to 1.73-1.75 eV with lowering of both the HOMO and LUMO levels.28 Fluorination within the aromatic backbone is not expected to affect the degradation pathway at the α-C found here. Although oxidation at the Sulphur site in the thiophene ring forming1 (O=S=O) or (S-O + C-O-H)29 has been suggested, it is not supported by the IR changes observed here. Unusual changes in IR absorption were also observed in reduced

graphene oxide following O-rearrangements to produce strongly IR-active modes of O bonded to edge atoms.[30]

We measured the wavelength dependent optical absorption and found no significant changes between pristine and light-degraded samples in N_2 or dry air (Fig. S5, ESI). Notably, degradation of organic solar cells may be caused by changes in additional layers (PEDOT:PSS, ITO etc.) and interfaces of OSCs, in additional to the absorber layer, and our work does not consider the effect of such additional layers/interfaces. . It is likely that photo-degradation in inert N2 is causing small bonding changes, below the measurement threshold of IR spectroscopy. Defect formation involving 1 in 104-105 atomic sites can only be observed through measurements of electronic sub-gap states or electron paramagnetic resonance (EPR). EPR measurements[19] of light-induced C-dangling bonds in polymer-fullerene blends with densities of 10^{18}-10^{19} cm^{-3} may be below IR detection threshold. The small magnitude of light-induced degradation is well-known in the realm of inorganic solar cells, where amorphous hydrogenated silicon (a-Si:H) exhibits light-induced metastability or the Staebler-Wronski effect.[31] The density of light-induced mid-gap electronic defects is ~10^{16}- 10^{17} cm-3, equivalent to changes involving 1 atom out of ~10^5.32-35 Such changes are exceedingly difficult to observe in IR spectroscopy, and can only be observed through subtle changes in the mid-gap electronic DOS or in electron spin resonance. In contrast, photo-structural changes in organic solar materials are orders of magnitude larger, and may affect a few % of all the atomic sites, as suggested by the new IR-active vibrational modes. This indicates fundamental differences between organic and inorganic materials. The lower stability of organic materials than inorganic, may be intimately related to the ease of carbon to form multiple bonding configurations and aromatic bonding configurations.

3.8 Conclusions

Photo-degradation is among the most pressing problems in organic electronics. We studied the photo-degradation of organic light-absorbing films (PTB7:PCBM) utilized in organic solar cells, performing infrared absorption spectroscopy on as-deposited and light-soaked films, in an environmental chamber under inert N_2 flow, with ambient air and dry air. Significant additional unexpected IR active absorption modes were found in PTB7:PCBM blends light soaked in the presence of oxygen (in ambient atmosphere and dry air), consisting of an intermediate frequency mode (1727 cm^{-1}) and a weak high frequency mode (3240 cm^{-1}). No significant IR changes were seen after light soaking in inert N2, or in ambient conditions in the dark. We interpret photo-degradation originating from the presence of oxygen and light, through the photoexcitation of the O_2 molecule from its triplet ground state to the excited singlet state (O_2*), that is well known to be very reactive.

To understand the atomistic pathways underlying this degradation we performed ab-initio density functional simulations. We found oxidation occurring at the α-C site of the alkyl side chains, forming a new C=O bond and a new C-O-H group at the α-C, accompanied by a rupture of the alkyl chains at the α-C site. This pathway accounts for the unusual measured increased strong absorption at 1727 cm^{-1} from the new C=O stretch mode, whereas the broad absorption at 3240 cm^{-1} is attributable to C-O-H stretch for hydroxyl groups at α-C. Organic polymers with bridging O may be substantially less photo-stable and our results offer pathways to designing more stable organic materials for solar cells and displays.

3.9 Supplementary Information

3.9.1. Anneal of PTB7:PCBM films for different anneal times:

(a) (b)

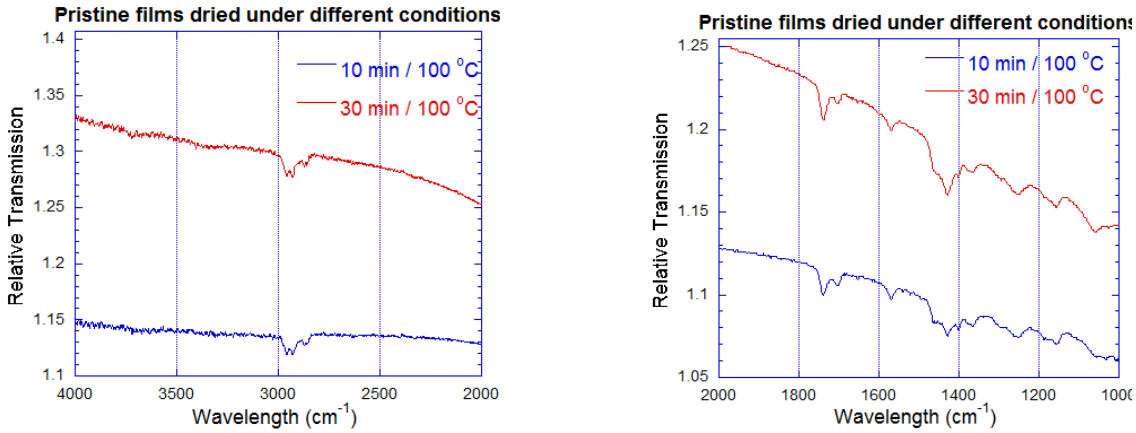

Fig. S1. Measured infrared (IR) transmission spectra of pristine PTB7:PCBM films that were annealed at 100 °C for 10 minutes (blue) and 30 minutes (red). The absorption is divided into a) high frequency (4000cm^{-1} to 2000cm^{-1}), and b) low frequency (2000cm^{-1} to 1000cm^{-1}).

3.9.2. Environmental chamber for light induced degradation studies.

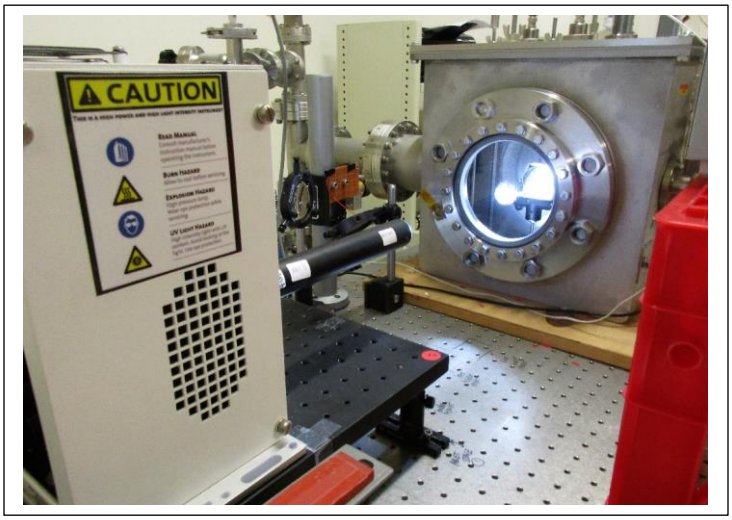

Fig. S2. Shown on the right side is the environmental chamber for measurement of light induced degradation of organic solar cell, that was filled with i) inert N_2 flow ii) dry air flow (N_2;O_2 70:30), or iii) ambient atmosphere (containing O_2 and moisture). Light is incident on a mirror inside the chamber that directs the light to the sample. The ABET solar simulator is on the left.

3.9.3. Infrared spectroscopy of PTB7 films (without the blend)

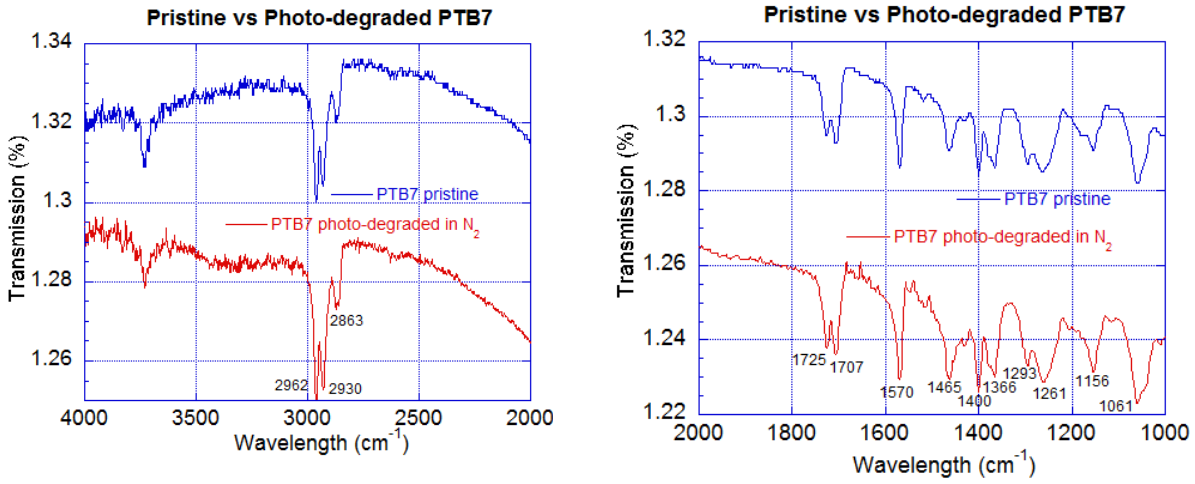

Fig. S2. Measured infrared (IR) transmission spectra of PTB7 film after photo-degradation in inert N_2 atmosphere. Pristine and photo-degraded film at a) high frequency (4000cm^{-1} to 2000cm^{-1}), and b) low frequency (2000cm^{-1} to 1000cm^{-1}).

Table S1. FTIR absorption features measured for pristine and photo-degraded (in N_2) PTB7 polymer films with the vibrational modes identified.

	pristine PTB7	**Photo degraded PTB7 in N_2**
Mode	Peak (cm^{-1})	Peak (cm^{-1})
CH2 asymm stretch	2960	2962
CH2 asymm stretch	2930	2933
CH2 symm stretch	2860	2862
C=O str. (aldehyde)	1725	1725
C=O str. (ester)	1707	1707
C=C aromatic str.	1570	1570
CH3 asym. bend	1465	1465
CF stretch	1400	1400
CH3 symm. bend	1366	1366
Asymm. C-O-C stretch+ CH2 twist	1293	1293
Asymm. C-O-C str; + CH2 twist	1261	1261
CH2 wag	1153	1153
C-O-C symm. stretch	1062	1066

In order to de-convolute the relative contributions of PTB7 and PCBM in the FTIR spectrum of the blend, we measured the absorption of PTB7 and PCBM films separately.

The PTB7 film in both pristine state and after light-degraded in N_2 shows (Fig. S2, Table S1) the stretch and bending vibrations similar to that in observed in the blend.Most of the IR-active modes observed in the PTB7:PCBM blend (Table 1), including the high frequency modes (above 2000 cm^{-1}), occur from the PTB7 component. No significant changes in absorption occur after light degradation in inert N_2, similar to the result observed with the blend.

3.9.4. Infrared spectroscopy of PCBM films (without the blend)

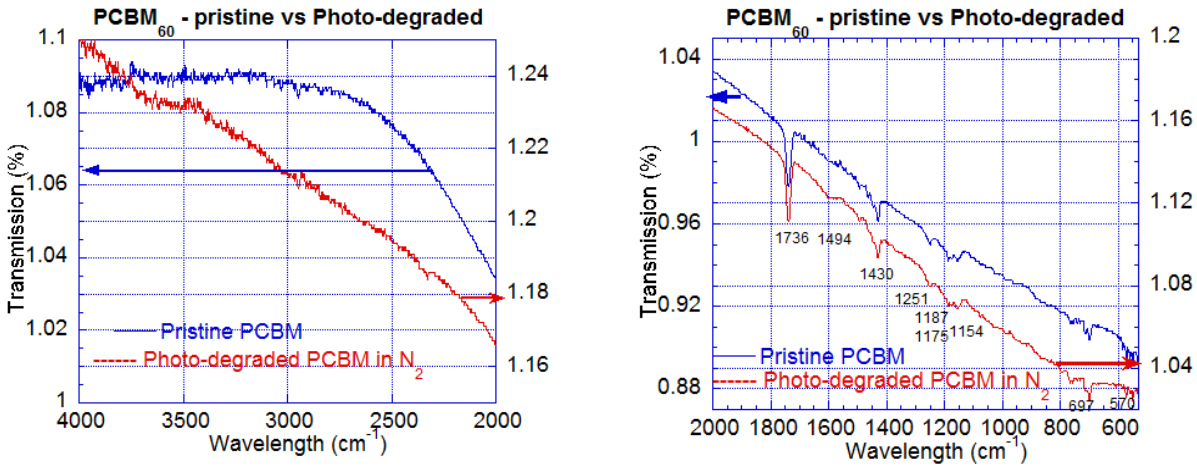

Fig. S3. Measured infrared (IR) transmission spectra of a PCBM film after photo-degradation in inert N_2 atmosphere. Pristine and photo-degraded film at a) high frequency (4000cm^{-1} to 2000cm^{-1}), and b) low frequency (2000cm^{-1} to 1000cm^{-1}).

The high frequency region (4000 – 2000 cm^{-1}) is featureless since there are very few ethyl (CH_2) groups in PCBM, compared to PTB7. At lower frequencies we observe C=O modes (1736 cm^{-1}), C-H bend (phenyl)(1494 cm^{-1}), CH_3 bend of the capping methyl group (1430 cm^{-1}), the C-H bend into the alkyl group (1251 cm^{-1}) and the C-O stretch modes of the

Table S2. FTIR absorption features measured for pristine and photo-degraded (in N_2) PCBM films with the vibrational modes identified.

	Pristine PCBM	**Photo degraded PCBM in N_2**
Mode	Peak (cm-1)	Peak (cm-1)
C=O str. (ester)	1736	1736
CH bend (phenyl)	1494	1494
CH_3 bend (methyl)	1430	1430
C-H bend (into alkyl)	1251	1251
C-O stretch (ester)	1187,1175,1154	1187,1175,1154
C-C stretch fullerene	697,570	697,570

ester group (1187,1175,1154 cm^{-1}) in both pristine and light degraded PCBM, similar to previous studies of PCBM (Ref. 28). We also observe the characteristic C-C fullerene modes of the C60 at 697 and 570 cm^{-1}.

3.9.5. Atomic configuration of the PTB7 monomer

Fig. S4. Atomic configuration of the PTB7monomer, with C(grey), H(white), O(red); S(yellow) and F(green). Lone pair electrons (pink) are shown. The monomer has been capped by H atoms at the two ends. The aromatic backbone (dashed) is connected to alkyl chains through O bridging atoms.

3.9.6. Optical Absorption spectrum

We measured the optical absorption of PTB7-PCBM blends before and after light-soaking in N_2 (Fig. S5 (a)); and before and after light-soaking in dry air (Fig. S5 (b). Negligible changes were observed. The band edge at 760 nm is consistent with the experimental band gap of 1.59 eV.

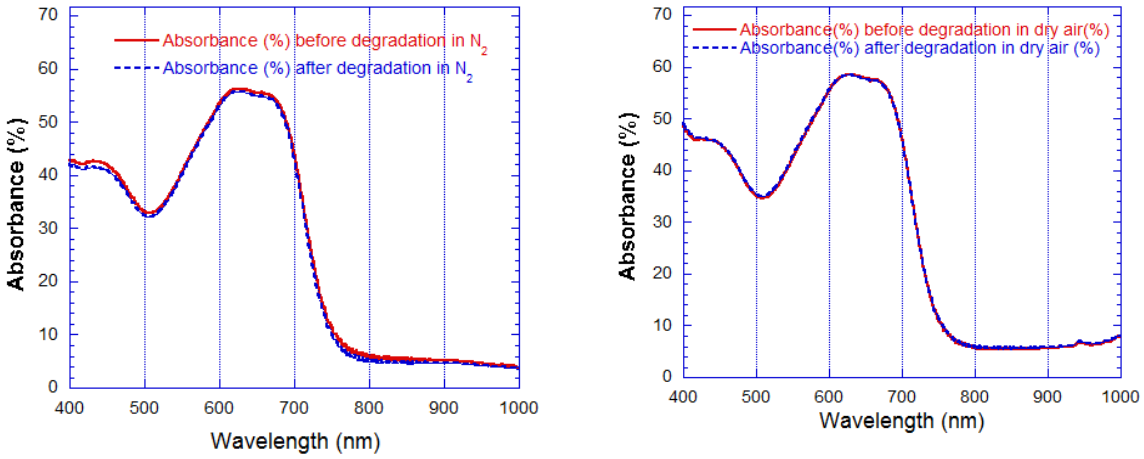

Fig. S5 The optical absorption of PTB7-PCBM blends a) before and after light-soaking in N2, and b) before and after light-soaking in dry air.

3.9.7. Analysis of photo-exposure of NaCl substrates

We examined the role of the NaCl substrate by photo-exposure of the bare substrates in ambient atmosphere (Fig. S6 (a,b)) and in dry air (Fig. S6 (c,d)), and comparing their IR absorption with the pristine salt substrate. No new IR absorption features were induced in the NaCl on photo-exposure. By plotting the ratios of the light exposed sample to the pristine sample, we observed an overall decrease of the IR transmission by ~ 8% after exposure to dry air (Fig. S6 (c) and between 0-10% for ambient atmosphere depending on the wavelength (Fig. S6 (d)).

(a) (b)

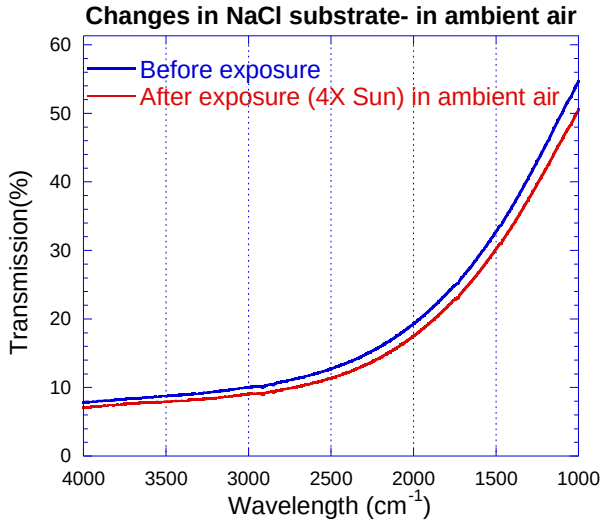

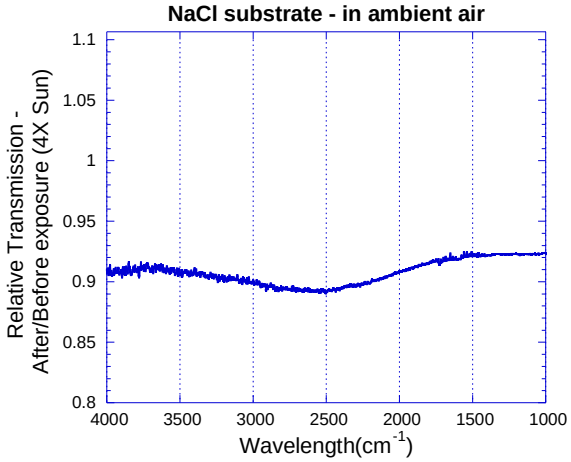

(c) (d)

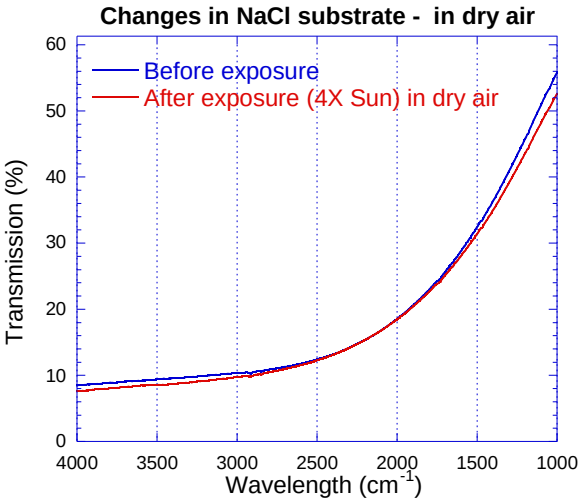

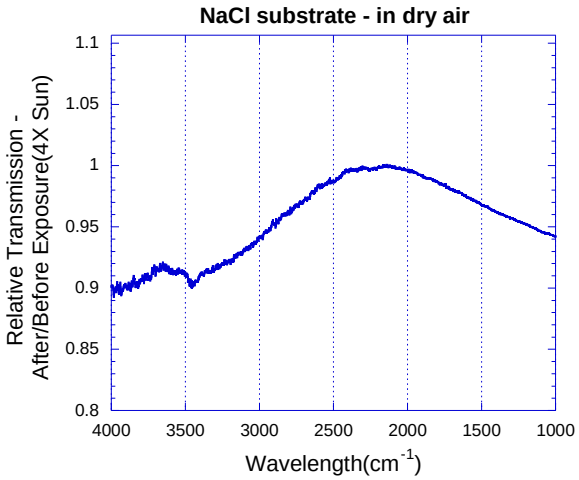

Fig. S6 a) Measured infrared (IR) transmission spectra of the bare uncoated substrate (NaCl) before light exposure (pristine) and after light exposure in ambient. b) Ratio of IR transmission of the photo-exposed in ambient and pristine NaCl. c) Measured infrared (IR) transmission spectra of the bare uncoated substrate (NaCl) before light exposure (pristine) and after light exposure in dry air. d) Ratio of IR transmission of the photo-exposed in dry air and pristine NaCl.

3.10 Acknowledgements

This work was supported (in part, R.B. and T.K.) by the U.S. Department of Energy (DOE), Office of Science, Basic Energy Sciences, Materials Science and Engineering Division. The research was performed at Ames Laboratory, which is operated for the U.S. DOE by Iowa State University under contract # DE-AC02-07CH11358. This work was supported (in part, S.S. and V.L.) by the National Science Foundation under grant CBET-1336134. We acknowledge use of computational resources at the National Energy Research Scientific Computing Center (NERSC) which is supported by the Office of Science of the USDOE under Contract No. DE-AC02-05CH11231.

3.11 Notes

P3HT, poly 3-hexylthiophene-2,5-diyl;

PCDTBT:PC70BM,poly[N-9'-heptadecanyl-2,7-carbazole-alt-5,5-(4',7'-di-2-thienyl-2',1',3'-benzothiadiazole)]:phenyl C70-butyric acid methyl ester;

PTB7, Poly({4,8-bis[(2-ethylhexyl)oxy] benzo[1,2-b:4,5-b′]dithiophene-2,6-diyl}{3-fluoro-2-[(2-ethylhexyl) carbon-yl]thieno [3,4-b]thiophenediyl}.

ITO, Indium tin oxide3.12 References

1. M. Jorgensen, K. Norman, and F. Krebs, Stability/Degradation of Polymer Solar Cells, *Solar Materials and Solar Cells* 2008, **92**, 686-714.

2. M. Jorgensen, K. Norman, S. Gevorgyan, T. Tromholt, B. An-dreasen, and F. Krebs, Stability of Polymer Solar Cells, *Ad-vanced Materials*, 2010, **24**, 580-612.

3. D. Yu, Y.-Q Yang, Z. Chen, Y. Tao, and Yun-Fei Liu,. Recent progress on thin-film encapsulation technologies for organic electronic devices, *Optics Communications*, 2016, **362**, 43–49.

4. X. Li, M. I. Dar, C. Yi, J. Luo, M. Tschumi, S. M. Zakeeruddin, M. K. Nazeeruddin, H.Han, and M. Grätzel,. Improved perfor-mance and stability of

perovskite solar cells by crystal crosslink-ing with alkyl phosphonic acid ω-ammonium chlorides, *Nature Chemistry* 2015, **7**, 703–711.

5. J. You et al, Improved air stability of perovskite solar cells via so-lution-processed metal oxide transport layers, *Nature Nanotechnology* 2016, **11**, 75-81.

6. R. A. Street, A. Krakaris, and S. R Cowan, Recombination through Different Types of Localized States in Organic Solar Cells, *Advanced Functional Materials*, 2012, **22**, 4608-4619.

7. C.H. Peters, I.T. Sachs-Quintana, J. P. Kastrop, S. Beaupre, M. Leclerc, and M. McGehee, High Efficiency Polymer Solar Cells with Long Operating Lifetimes, *Adv. En. Mat.* 2011, **1**, 491-494.

8. J. Bhattacharya, R. W. Mayer, M. Samiee, and V. L. Dalal, Photo-induced Changes in Fundamental Properties of Polymer Solar Cells, *Appl. Phys. Lett.* 2012, **100**, 193501.

9. Q. Burlingame, X. Tong, J. Hankett, M. Slootsky, Z. Chen, S. Forrest, Photochemical Origins of Burn-in Degradation in Small Molecular Weight Organic Photovoltaic Cells, *Energy Env. Sci.* 2015, **8**, 1005-1010.

10. H.C. Wong, Z. Li, C.H. Tan, H. Zhong, Z. Huang, H. Bronstein, I. McCulloch, J.T. Cabral, and J.R. Durrant, Morphological Stability and Performance of Polymer Fullerene Solar Cells under Thermal Stress: The Impact of Photoinduced PC60BM Oligomerization, *ACS Nano* 2014, **8**, 1297-1308.

11. A. Guerrero, H.Heidari, T. S. Ripolles, A. Kovalenko, M. Pfannmöller, S. Bals, L-D. Kauffmann, J. Bisquert, and G. Garcia-Belmonte, *Adv. En. Mat.* 2015, **5**, 1401997.

12. T. Xiao, F. Fungara, M. Cai, J.W. Andreeg, J. Shinar R. Shinar, Improved efficiency and stability of inverted polymer solar cells with a solution-processed BPhen interlayer and polystyrene beads, *Org. Electron.* 2013, **14**, 2555-2563.

13. R. Street, J. Northrup, B.J. Krusor, Radiation Induced Recombination Centers in Organic Solar Cells, *Phys. Rev. B.* 2012, **85**, 205211.

14. Y. Zhang, E.Bovill, J.Kingsley, A. R. Buckley, H. Yi, A. Iraqi, T. Wang, and D.G. Lidzey, PCDTBT based solar cells: one year of operation under real-world conditions, *Scientific Reports* 2016, **6**, 21632.

15. D. H. Wang, J. K. Kim, J. H. Seo, O. O. Park, and J. H. Park, Stability comparison: A PCDTBT/PC71BM bulk-heterojunction vs a P3HT/PC71BM bulk-heterojunction, *Solar. En. Mat. & Solar Cells* 2012, **101**, 249-255.

16. J. Razzell-Hollis, J. Wade. W.C. Tsoi, Y. Soon, J. Durrant, and J.-S.Kim, Photochemical stability of high efficiency PTB7:PC70BM solar cell blends, *J. Materials Chem. A* 2014, **2**, 20189-20195.

17. M.B. Arredondo, B. Martin-Lopez, R. Romero, R. Vergaz, P. Romero-Gomez, and J. Martorell, Monitoring degradation mechanisms in PTB7:PC71BM photovoltaic cells by means of impedance spectroscopy, *Sol. En. Mat. & Solar Cells*, 2016, **144**, 422-428.

18. J. Northrup, Radiation Induced Hydrogen Rearrangement in Poly(3-alkylthiophene), *Applied Physics Express* 2013, **6**, 121601.

19. F. Fungara, W.H. Lindemann, J. Shinar, and R. Shinar, Carbon dangling bonds in photodegraded polymer:fullerene solar cells, *Adv. Func. Materials* 2016, 1601420.

20. Y. W. Soon, H. Cho, J. Low, H. Bronstein, I. McCulloch, and J. R. Durrant, Correlating triplet yield, singlet oxygen genera-tion and photochemical stability in polymer/fullerene blend films, *Chem. Commun*., 2013, **49**, 1291—1293.

21. S. Shah, and R. Biswas, Fundamental atomic mechanisms underlying intrinsic degradation in organic solar cell materials, *J Physical Chemistry C*, 2015, **119** (35), 20265–20271.

22. Barbara H. Stuart, Infrared Spectroscopy: Fundamentals and Applications, (John Wiley and Sons, 2004).

23. http://chemwiki.ucdavis.edu/Reference/Reference_Tables/Spectroscopic_Parameters/Infrared_Spectroscopy_Absorption_Table.

24. J. M. Soler, E. J. Artacho, D. Gale, A. Garcia, J. Junquera, P. Ordejon, and D. Sanchez-Portal, The SIESTA Method for ab-initio Order-N Materials Simulation, *J. Phys. Condens. Matter* 2002, **14**, 2745-2779.

25. N. Troullier, and J. L. Martins, Efficient Pseudopotentials for Plane-wave Calculations, *Phys. Rev. B* 1991, **43**, 1993-2006.

26. J. P. Perdew, M. Ernzerhof, and K. Burke, Rationale for Mixing Ex-act Exchange with Density Functional Approximations, *J. Chem. Phys.* 1996, **105**, 9982-9985.

27. H. J. Son, W. Wang, T. Xu, Y. Liang, Y. Yue, G. Li, and L. Yu, Synthesis of fluorinated polythienothiophene -co-benzodithiophenes and effect of Fluorination on the Photovoltaic Properties, *J. Am Chem Soc.* 2011, **133**, 1885-1894.

28. M. Acik, G. Lee, C. Mattevi, M. Chhowalla, K. Cho, and Y. J. Chabal, Unusual infrared-absorption mechanism in thermally re-duced graphene oxide, *Nat. Mater.* 2010, **9**, 840-845.

29. D. L. Staebler, and C. R. Wronski, Reversible Conductivity Changes in Discharge-produced Amorphous Si, *Appl. Phys. Lett.* 1977, **31**, 292-294.

30. M. Stutzmann, W. Jackson, and C.C. Tsai, Light-induced metastable defects in hydrogenated amorphous silicon: A sys-tematic study, *Phys. Rev. B.* 1985, **32**, 23-42.

31. H. R. Park, J. Z. Liu, and S. Wagner, Saturation of the light-induced defect density in hydrogenated amorphous silicon, *Appl. Phys. Lett.* 1989, **55**, 2658-2661.

32. R. Biswas, Q. Li, B.C. Pan, and Y. Yoon, Mechanism for hydrogen diffusion in amorphous silicon, *Phys. Rev. B.* 1998**, 57**, 2253-2258.

33. R. Biswas, B.C. Pan, and Y. Ye, Metastability of amorphous silicon from silicon network rebonding, *Phys. Rev. Lett.* 2002, **88**, 205502-205505.

CHAPTER 4. IDENTIFICATION OF DEGRADATION PATHWAYS OF ORGANIC SOLAR CELLS USING INFRARED SPECTROSCOPY

S. Shah[1] and R.Biswas[1,2,3], T. Koschny[2], and V L Dalal[1]

1. Microelectronics Research Center, and Department of Electrical Engineering, Iowa State University, Ames, IA 50011-3060
2. Ames Laboratory, Ames –Iowa 5001-3060
3. Dept. of Physics, Iowa State University, Ames, IA 50011-3060

Adapted from an article published in *IEEE – PVSC Proceedings* no. 698(2017)

4.1 Abstract

The degradation of organic solar cells is one of the most urgent problems facing further scientific and commercial development of organic electronics. Degradation can occur in the presence of light exposure together with external oxygen and moisture. We utilize infrared (IR) spectroscopy to identify IR active vibrational modes and the atomistic changes occurring during degradation of organic solar cell films, before and after degradation. We find measurable changes when light exposure is performed in the presence of oxygen or an ambient environment. The low band gap PTB7-PCBM blend films display significant increases of increased absorption at 1727 cm^{-1} attributable to increased C=O modes in conjunction with a broad increase at 3240 cm^{-} attributed to hydroxyl (OH) groups within polymer. Ab-initio modeling indicates that this can be explained by an oxidation of the PTB7 polymer at the α-C site and a irreversible cleaving of the polymer. Light induced degradation performed in the absence of oxygen/moisture do not lead to large changes in the IR active modes. P3HT-PCBM

blends do demonstrate small changes around 2500 cm^{-1} after light soaking, that may be connected to local H-motion induced rearrangements. Films exposed to the ambient atmosphere in the dark do not show IR active changes, identifying photo-excited singlet oxygen to be detrimental. The identification of light induced changes in atomic bonding configurations can open up pathways to stabilizing organic solar cells.

4.2 Introduction

Organic photo-voltaics (OPVs) have great promise as a platform for simple, low cost, flexible solar cells. One of the primary roadblocks preventing commercial deployment of OPVs is the instability of the OPVs during light exposure. Stability issues also plague the newly discovered perovskite materials. It is of great interest to assess whether photo-degradation can be reversible or irreversible.

Many studies have reported the photo-degradation of organic solar cells, including the loss of short circuit current (J_{sc}), open circuit voltage (V_{oc}), fill factor (FF) and efficiency (η) after light soaking in inert ambient environments [1,2]. Measurements of mid-gap states in films found distinct increases in mid-gap densities of states with light and UV exposure, with a hint of stabilization at long time [3]. The oxidation of conjugated vinylene groups has been well studied [1,4] and detailed measurements have identified the diffusion of metal from the cathode, as well as In from the the ITO contact, as potential sources of degradation. Hole-transport layers such as PEDOT:PSS and the various interfaces in OSC's have been suggested to cause instability [1,4].

To avert the complexity in dealing with the various interfaces, and electron- and hole-transport layers in OSCs, we focus on the stability of the intrinsic absorber layer alone in this paper. Changes in device architecture such as use of inverted OScs cannot alter the behavior

of the absorber layer. In our approach we deposit organic absorber layers on standard substrates using identical processing conditions used in the fabrication of solar cells. Thus for done-acceptor blends we expect the same bulk hetero-structure in films that were present in devices. There have been very few studies for understanding the atomistic changes occurring after light-degradation. We utilize infrared spectroscopy as the technique for identifying changes in atomic bonding species after light-induced degradation.

4.3. Experimental Details

We spin coat organic films on salt (NaCl) substrates, which are transparent within the large window from 4000 to 650cm^{-1}. In contrast standard silicon wafers transmit less than ~60% in the mid-IR and suffer from Fabry-Perot fringes that compromise sensitivity. We chose for our studies i) the low band gap polymer PTB7 that is frequently used as a donor in higher efficiency OSCs with efficiency exceeding 8%, ii) P3HT the most common prototypical done used in OSCs with 3-4% efficiency iii) The common acceptor PCBM60 and iv) donor-acceptor blends of PTB7:PCBM60 and P3HT:PCBM60.

Synthesis of PTB7:PCBM60 blend films were prepared with a solution of PTB7 (1-Material, 10 mg) and PCBM60 (Nano-C, 15 mg) in dichlorobenzene solvent (Sigma Aldrich, 0.97 mL) and 1,8-Diiodooctane (DIO) additive (Sigma Aldrich, 0.03 mL (i.e. 3%) in a glove box that was stirred for 12 hours at 75 °C and 300 rpm. The blend was spin-coated on NaCl substrates at 600 rpm for 60s. The sample was then dried at 100 °C for 30 minutes on a hot-plate, to achieve a film thickness of ~100nm nm, typical of absorber layers in OSCs. Spin-coating and drying were performed in a nitrogen filled glove box where H_2O and O_2 levels

were a few ppm. For these deposition conditions the film thickness was ~100 nm, typical of the absorber layer in PTB7 solar cells.

Light soaking was performed with an ABET solar simulator capable of 1x to 4x solar-intensity variation. The light soaking was performed inside an environmental chamber with i) an inert N_2 flow ii) dry air containing a mixture of 70:30 N_2/O_2 and iii) ambient air atmosphere containing both O2 and moisture.

Fourier transform infrared spectroscopy (FTIR) was carried out in vacuum with a Bruker Vertex 70v spectrometer in which the NaCl samples were placed in an evacuated sample chamber. Reference measurements were performed with i) no sample and ii) salt substrate (without any film). The transmission of pristine (as-deposited) films was measured on the same substrate. The films were then light soaked and the IR transmission re-measured utilizing the bare salt as the reference.

4.4. Results

IR spectroscopy is a technique with a sensitivity of a percent to a fraction of a percent. IR is not expected to measure changes below such a threshold. It should be recognized that in device measurements density of electronic states changes after light soaking are in the range of 1017 cm^{-3}, or 1 atom in 105 and cannot be observed in IR measurements.

We performed IR spectroscopy of pristine and light-soaked PTB7 films, and PTB7:PCBM blends that were light soaked in N_2, ambient air and dry air in a mixture of 70:30 N_2:O_2. In addition we kept films in the dark in an ambient air atmosphere for one week in the dark and reexamined their IR absorption spectra. The largest measurable changes in the IR

absorption were observed in films that were light soaked in dry air or in the ambient atmosphere. Since no measurable changes were observed for films in the dark we concluded that oxygen or moisture alone does not cause degradation. Instead it is necessary to have a combination of oxygen and light. The likely interpretation of this is that light excites triplet oxygen molecules to its excited singlet state (O_2*), which in turn can oxidize or react with organic species. Table 1 qualitatively summarizes these findings

Table 1: General observations with IR spectroscopy

Procedure	**Effect**
Light soak in N_2	Small IR changes
Light soak in N_2:O_2	IR absorption changes
Light soak in ambient air	IR absorption changes
Exposed to ambient in dark	No significant change

The significant measurements (Fig. 1) show the IR absorption spectrum for PTB7 pristine film compared with the film exposed in 2x solar intensity for 24 hours. Both films display the high frequency asymmetric and symmetric CH2 stretch vibration modes at 2960 and 2933 cm^{-1}, accompanied by the CH stretch from the conjugated back bone at 2867 cm^{-1}. There is a new broad absorption near 3240 cm-1 for the light degraded case. There are few species that can contribute to such a high frequency mode. The only viable species is the hydroxyl O-H group, with the OH group bonded within the organic backbone [5], since free water (H_2O) has OH vibrations at higher frequency (3500-3700 cm^{-1}). Although NH vibrations

also lie in this range, N is and amine groups are not present in the organic matrix and can be ruled out.

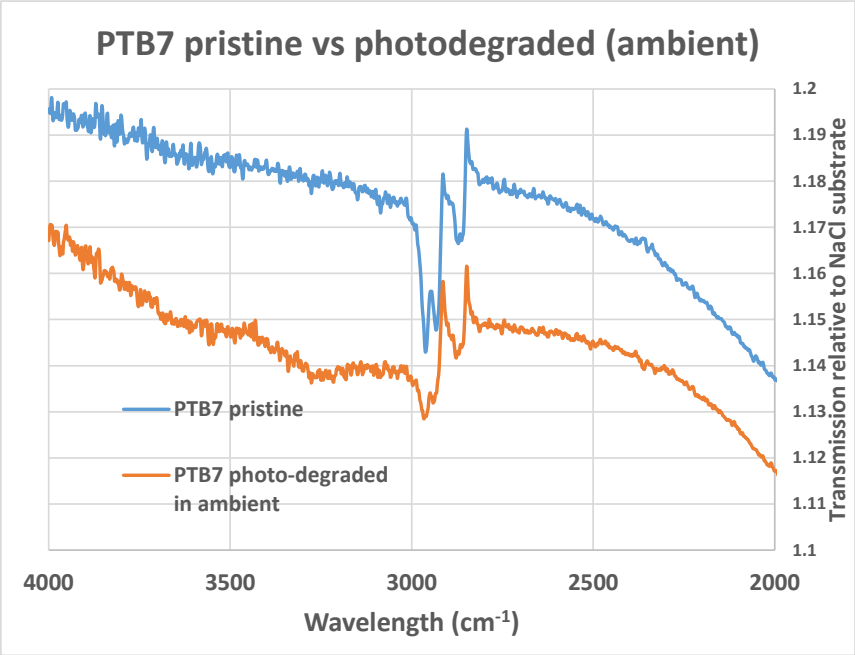

Fig. 1. Measured high-frequency infrared (IR) transmission spectra of PTB7 film showing the pristine as-deposited and photo-degraded film in ambient air atmosphere.

The low frequency IR absorption (Fig. 2) is considerably more complex, having the principal features of C=O stretch (1733 cm^{-1}), CH_3 asymmetric bend (1456 cm^{-1}), CH_2 scissor bend (1431cm^{-1}), C-O-C stretch (1061 cm^{-1}). CH_2 wag (1153 cm-1). In the film photodegraded in ambient, many of the lower frequency features are bleached away. The noticeable change is the strengthening of the 1727 cm^{-1} mode, which we interpret as increased C=O bond density.

In contrast we light soaked PTB7 films in an inert N_2 atmosphere (Fig. 3) and found only minor changes in the IR spectrum over all frequency ranges. This argues for the presence of light and oxygen to be important for such degradation effects.

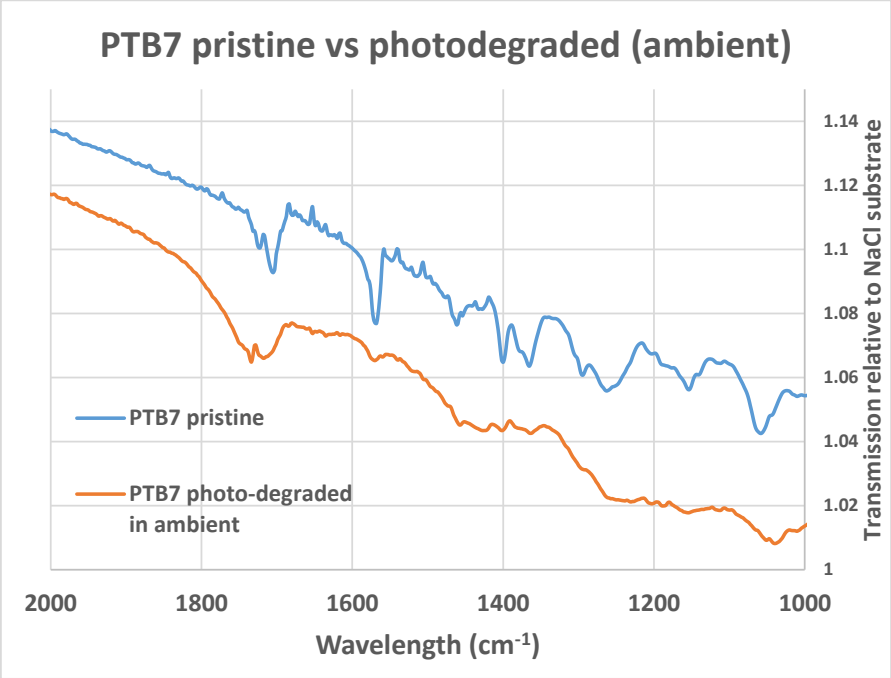

Fig 2. Measured low-frequency infrared (IR) transmission spectra of PTB7 blend films showing the pristine as-deposited and photo-degraded film in ambient air atmosphere.

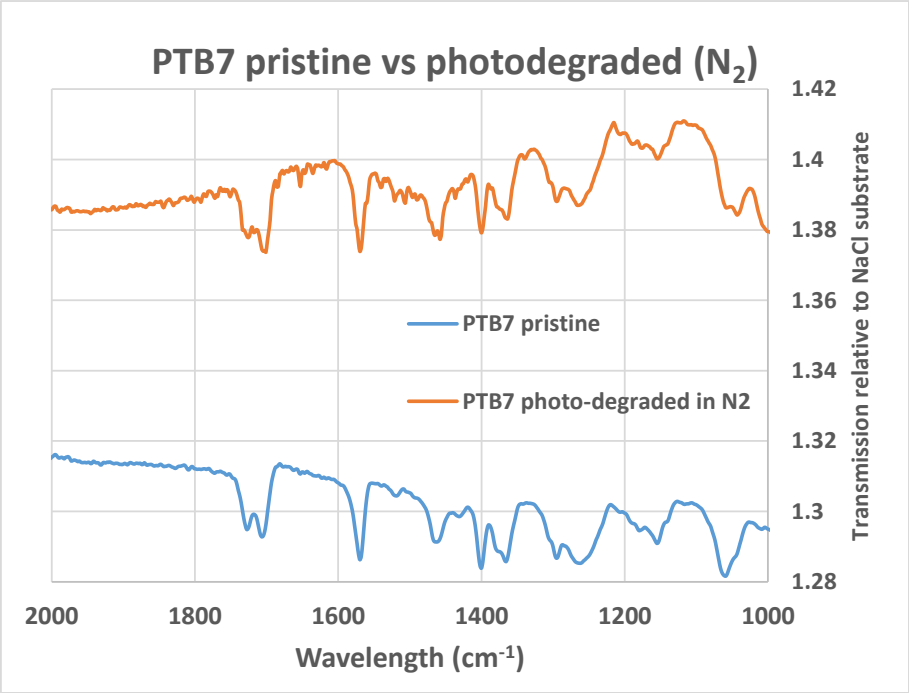

Fig. 3. Measured low-frequency infrared (IR) transmission spectra of PTB7 films showing the pristine as-deposited and photo-degraded film in an inert N_2 atmosphere.

The microscopic interpretation of these changes is based on our ab-initio simulations [6] of the PTB7 polymer. PTB7 consists of an aromatic backbone attached to polymer side-chain through a bridging O atom (Fig. 4). It is well known that the most reactive C site is α-C, the first C in the polymer chain. Our ab-initio simulations identify external O_2 as reacting with α-C forming a O=αC-O-H species. This increases the C=O stretch and creates a broad OH based absorption near 3240 cm^{-1}. The PTB7 polymer cleaves at the αC site – which is likely an irreversible change. Polymers with such a bridging O atom can exhibit such instability.

Fig. 4 Atomic structure of the PTB7 polymer with the αC site marked.

We did observe an interesting but small change in the IR absorption of P3HT:PCBM (Fig. 5). Since there is no bridging O there are fewer modes which do include the CH2 stretch 2800-2900 $cm^{-1}$and CH_2 bend modes below 1800 cm^{-1}. After light soaking in N_2, there is a small increase in absorption at 2400 cm^{-1}, with negligible changes in other portions of the spectrum.

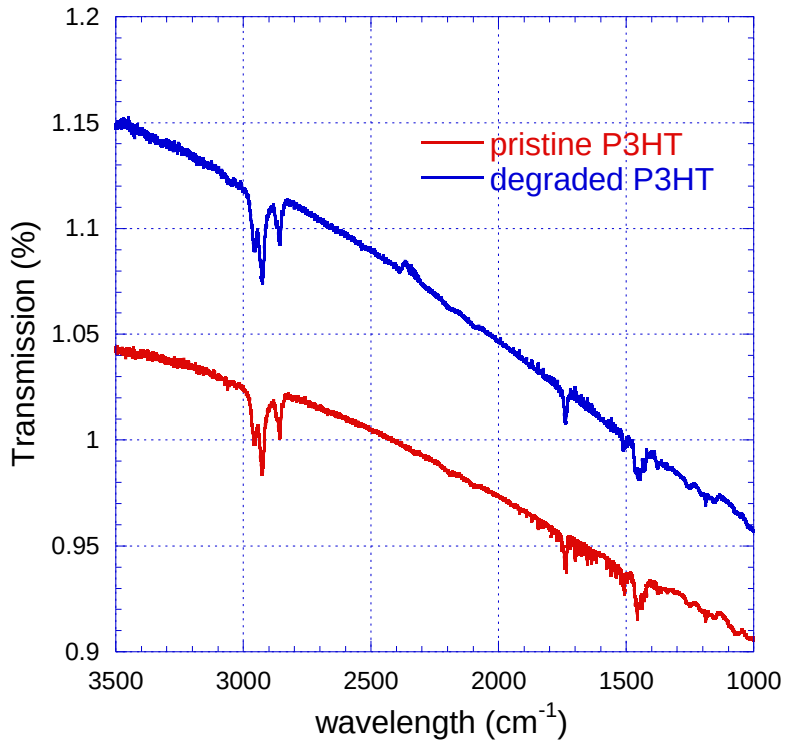

Fig. 5 IR transmission spectra of P3HT:PCBM in the pristine state and light soaked in Nitrogen.

It is likely that the feature at 2400 cm-1 may be caused by motion of H from the αC to within the thiophene ring, as suggested in earlier ab-initio simulations by Northrup et al [7] and also examined by us [8].

It is of great interest to characterize the minimum wavelength i.e. the minimum energy of the photons responsible for such degradation effects. Previous theoretical studies [8] place it in the blue wavelengths and future work will quantitatively explore this.

4.5. Conclusion

We have utilized infrared spectroscopy to identify atomic bonding changes occurring after light-degradation of organic absorber films. The largest oxidative changes are observed after light-soaking in ambient air or dry air and involve new C=O and O-H modes in the material. Subtle changes in H bonding may be observed in light-degradation of P3HT-PCBM.

4.6 Acknowledgement

This work was supported in part (RB, TK) by the U.S. Department of Energy (DOE), Office of Science, basic Energy Sciences, Division of Materials Science and Engineering. Ames Laboratory is operated for the U.S. DOE by Iowa State University under contract No. AC02-07CH1135. This work was also supported in part (SS and VLD) by the National Science Foundation under grant CBET-1336134 and (SS) CMMI-1265844. We acknowledge use of computational resources at the National Energy Research Scientific Computing Center (NERSC) which is supported by the Office of Science of the USDOE under Contract No. DE-AC0205CH11231.

4.7 References

[1] Jorgensen, M.; Norman, K.; F. Krebs, F.; Stability/Degradation of Polymer Solar Cells, Solar Materials and Solar Cells 2008, 92, 686-714.

[2] Bhattacharya, J.; Mayer, R. W.; Samiee, M.; and Dalal, V. L., Photo-induced Changes in Fundamental Properties of Polymer Solar Cells, Appl. Phys. Lett. 2012, 100, 193501.

[3] Street, R. A.; Krakaris, A.; and Cowan, S. R, Recombination through Different Types of Localized States in Organic Solar Cells, Advanced Functional Materials, 2012, 22, 4608-4619.

[4] Jorgensen, M.; Norman, K.; Gevorgyan, S.; Tromholt, T.; Andreasen, B.; Krebs, F.; Stability of Polymer Solar Cells, Advanced Materials, 2010, 24, 580-612.

[5] Barbara H. Stuart, Infrared Spectroscopy: Fundamentals and Applications, (John Wiley and Sons, 2004).

[6] S. Shah, R. Biswas, T. Koschny, and V. Dalal, Unusual Infrared Changes in Organic Polymer Films, Nanoscale **9**, 8665-8673 (2017).

[7] J. Northrup, Radiation Induced Hydrogen Rearrangement in Poly(3-alkylthiophene), Appl. Phys. Express **6** (2013) 121601.

[8] S. Shah, and R. Biswas, Fundamental atomic mechanisms underlying intrinsic degradation in organic solar cell materials, J Physical Chemistry C, **119** (35), 20265–20271 (2015).

CHAPTER 5. STABILITY OF DEUTERATED ORGANIC SOLAR CELLS

5.1 Introduction

The photo-degradation of organic solar cells and especially P3HT:PCBM solar cells has been well studied. Most studies find the cause of device degradation to be the degradation of the absorber layer itself – the donor P3HT polymer or the acceptor PCBM60 molecule. Not only is the polymer known to degrade in presence of moisture and air, but also mechanisms have been proposed for its photo-induced degradation.

Northrup has suggested a mechanism based on migration of alpha-H atom from the alkyl chains of the P3HT polymer to the thiophene rings creating defects and hence degrading the solar cell performance. The mechanism involves breaking away of the α-H atom with a simultaneous motion towards the thiophene ring, finally attaching itself to a C atom inside the ring (Fig. 1).

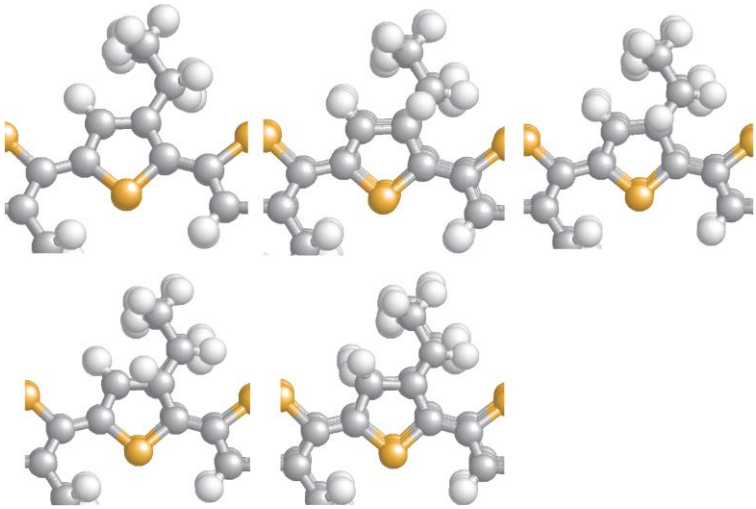

Fig. 1 Motion of H from a-C to the thiophene ring from simulations.

If the α-H atoms play an important role in the degradation mechanism, then we should look at the degradation of performance when these α-H atoms are replaced by Deuterium

atoms. The kinetic isotopic effects suggest that the degradation of the polymer might be very different for this new, deuterium substituted polymer.

In this light, we synthesized a polymer similar to P3HT, replacing only the 2 α-H atoms with deuterium atoms, D (fig. 1) with high yield. This polymer, henceforth referred to as P3HT-d_2, was then used to fabricate solar cells.

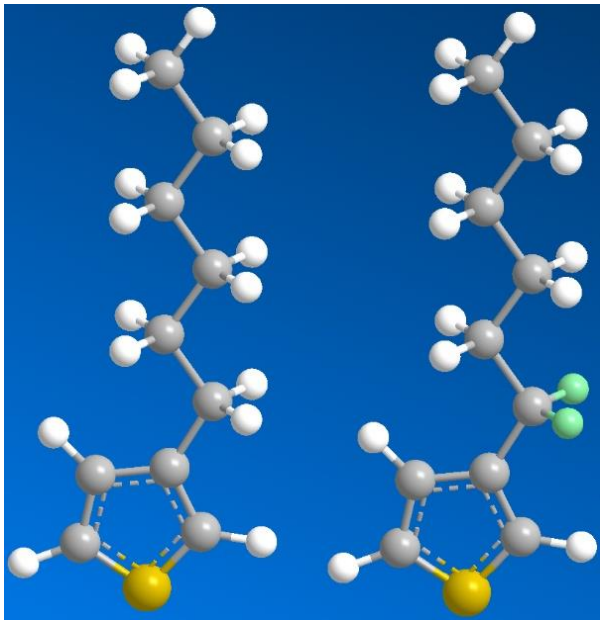

P3HT P3HT-d2

Fig. 2 Comparison of P3HT and deuterated P3HT, where D substitutes both H on the α-C site

The solar cell device structure is Glass/ITO/PEDOT:PSS/P3HT-d2:PCBM60/Ca/Al (fig). Under identical conditions, two sets of solar cells were fabricated, one using the standard P3HT polymer and another using our P3HT-d2 polymer (Solar cell fabrication parameters & procedure indicated at the end).

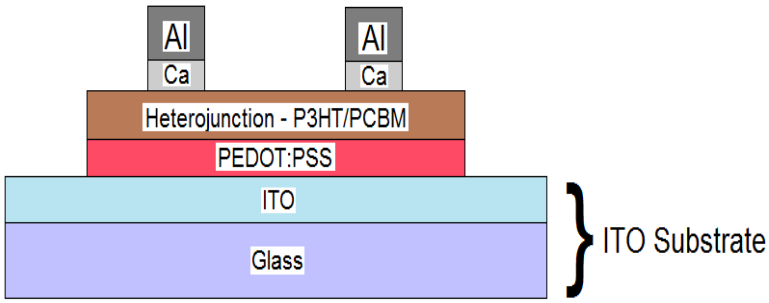

Fig. 3 Schematic device structure fabricated for organic solar cell

5.2 Results

5.2.1 Characterization

The fabricated solar cells were characterized using standard techniques.

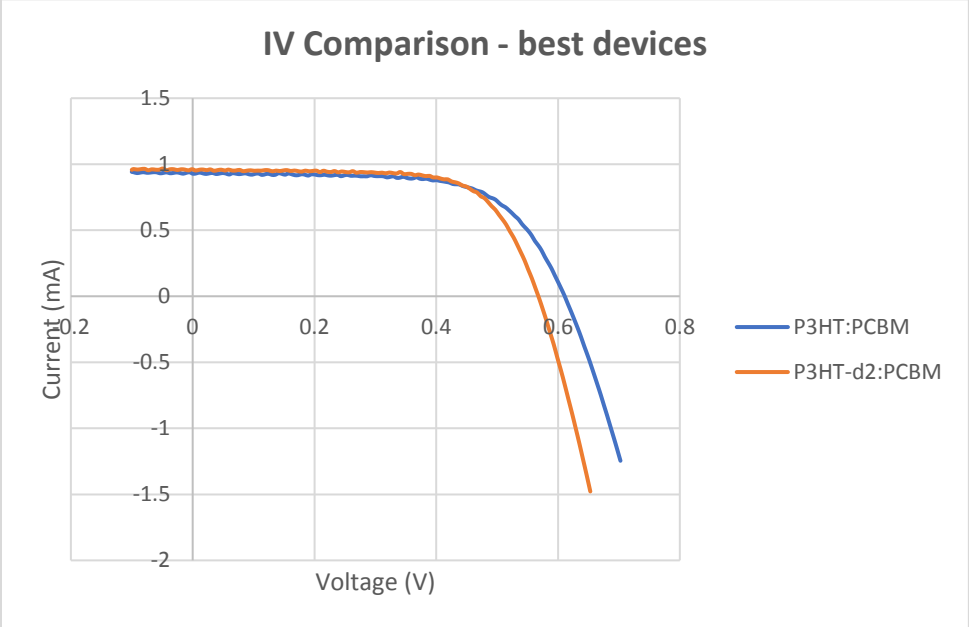

Fig. 4 Illuminated I-V curves for (a) P3HT-d2:PCBM BHJ solar cell; and (b) P3HT:PCBM BHJ solar cell

Subtracting the shunt current from this total current and fitting an exponential of the form $I = I_o \exp(qV/nKT)$ yields the reverse saturation currents and the combined ideality factor n for the diode. Using these we can calculate the V_{oc} from, $V_{oc} = nKT \ln(I_{sc}/I_o)$.

Table 1: Comparison of device characteristics for P3HT and deuterated P3HT cells

Polymer	Voc	Jsc	Fill Factor	Efficiency
P3HT	0.61 ± 0.00	0.92 ± 0.02	64.9 ± 0.9	3.44 ± 0.06
P3HT-d2	0.57 ± 0.00	0.92 ± 0.02	69.2 ± 0.7	3.43 ± 0.05
P3HT(best)	0.61	0.93	66.2	3.54
P3HT-d2(best)	0.57	0.96	68.2	3.52

Format: Average ± Standard Deviation

(Over 12 devices)

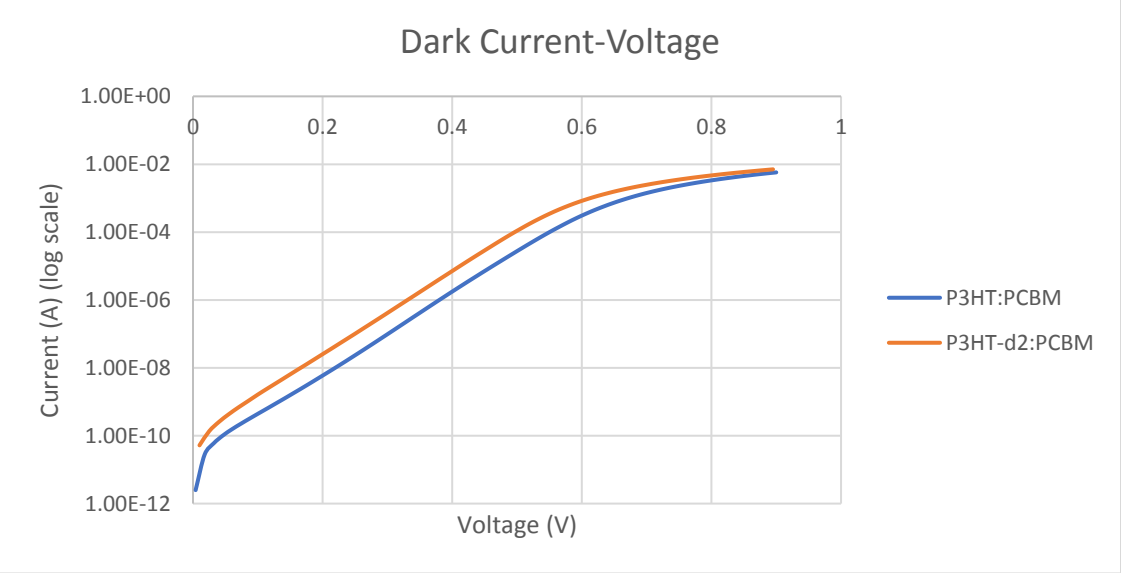

Fig. 5 Dark IV is plotted as a standard semi-log plot.

Table 2: Dark I-V characteristics for P3HT and deuterated P3HT cells

Polymer	Reverse saturation current Io (A)	Ideality factor (n)	Calculated Voc (V)
P3HT	1.7E-11	1.33	0.62
P3HT-d2	8.0E-11	1.35	0.57

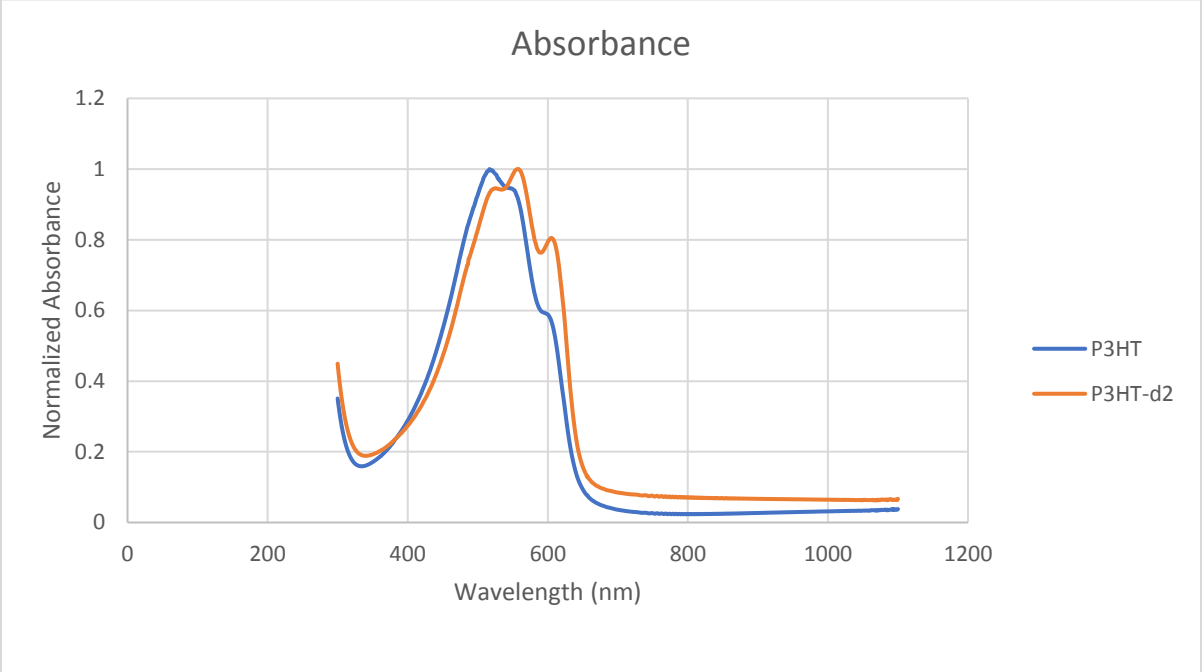

Fig. 5 Comparison of absorbance for P3HT and deuterated P3HT films

It has been shown that the density of states at a given energy is proportional to C(dC/df). Hence we can measure the density of defects within the band-gap using capacitance-frequency (C-f) measurements. The density of states distribution is similar in shape for P3HT and P3HT-d2 based devices with a minimum around 0.45 eV from the LUMO. The magnitude of defects is slightly higher for P3HT-d2 based device which can be explained by lower crystallinity or more disordered arrangement of P3HT-d2:PCBM mixture as indicated by sharper peaks in a comparison of QE data.

In the absorber layer, the electrons are collected by PCBM and the holes by the polymer (P3HT). Hence the hole mobility is an important parameter for any polymer used as donor in a bulk heterojunction organic solar cell. We found similar SCLC hole mobility: - 1.9E-04 cm^2/V-s for P3HT and 1.6E-04 cm^2/V-s for P3HT-d2. (Procedure indicated at the end)

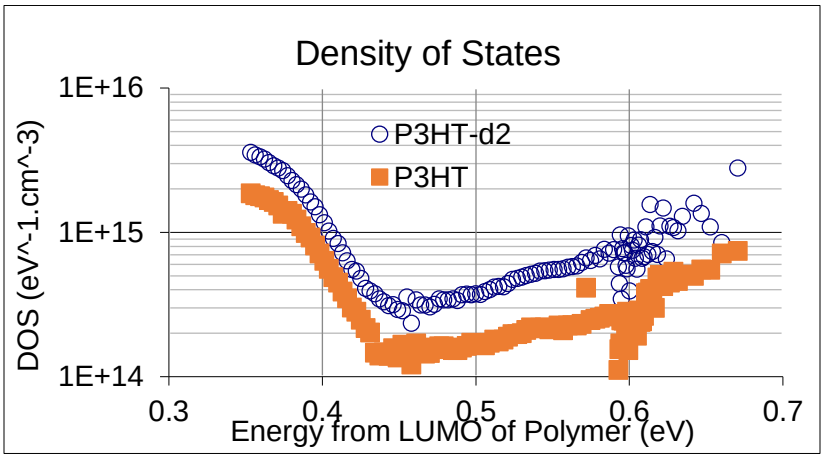

Fig. 6. Comparison of electronic densities of states for P3HT and deuterated P3HT films

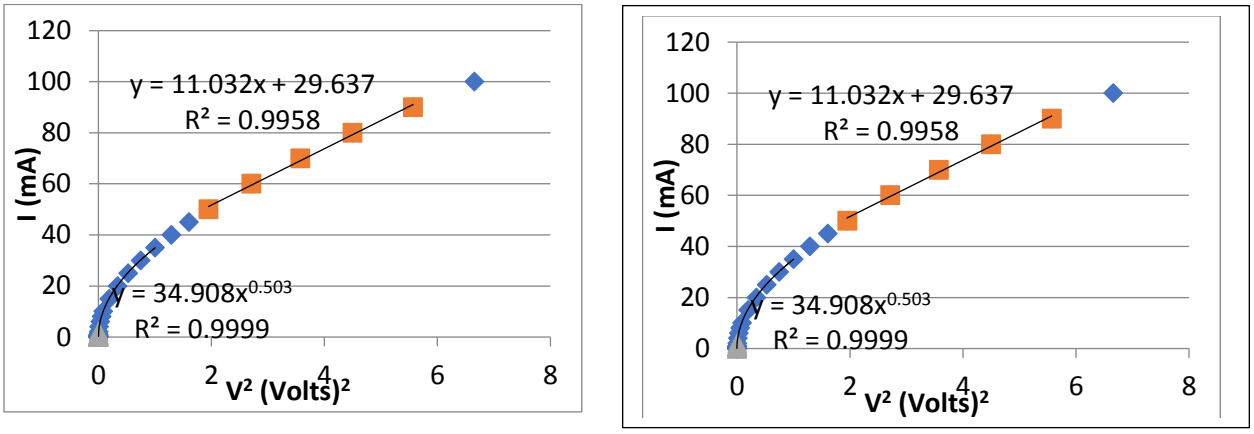

P3HT P3HT-d2

Fig. 7 Comparison of hole-mobility for P3HT and deuterated P3HT films

5.2.2 Degradation

Surprisingly, P3HT-d2 based solar cell shows a considerably faster degradation in comparison to standard P3HT based solar cell. (Degradation parameters and procedure indicated in detail at the end). While V_{oc} reduces by about 1%, J_{sc} by 5% and PCE by 3-4% for P3HT based solar cell, for the P3HT-d2 based solar cell V_{oc} reduces by about 4%, J_{sc} by 4-5% and PCE by 13%. These results clearly establish the important role of α-H atoms in the degradation mechanism.

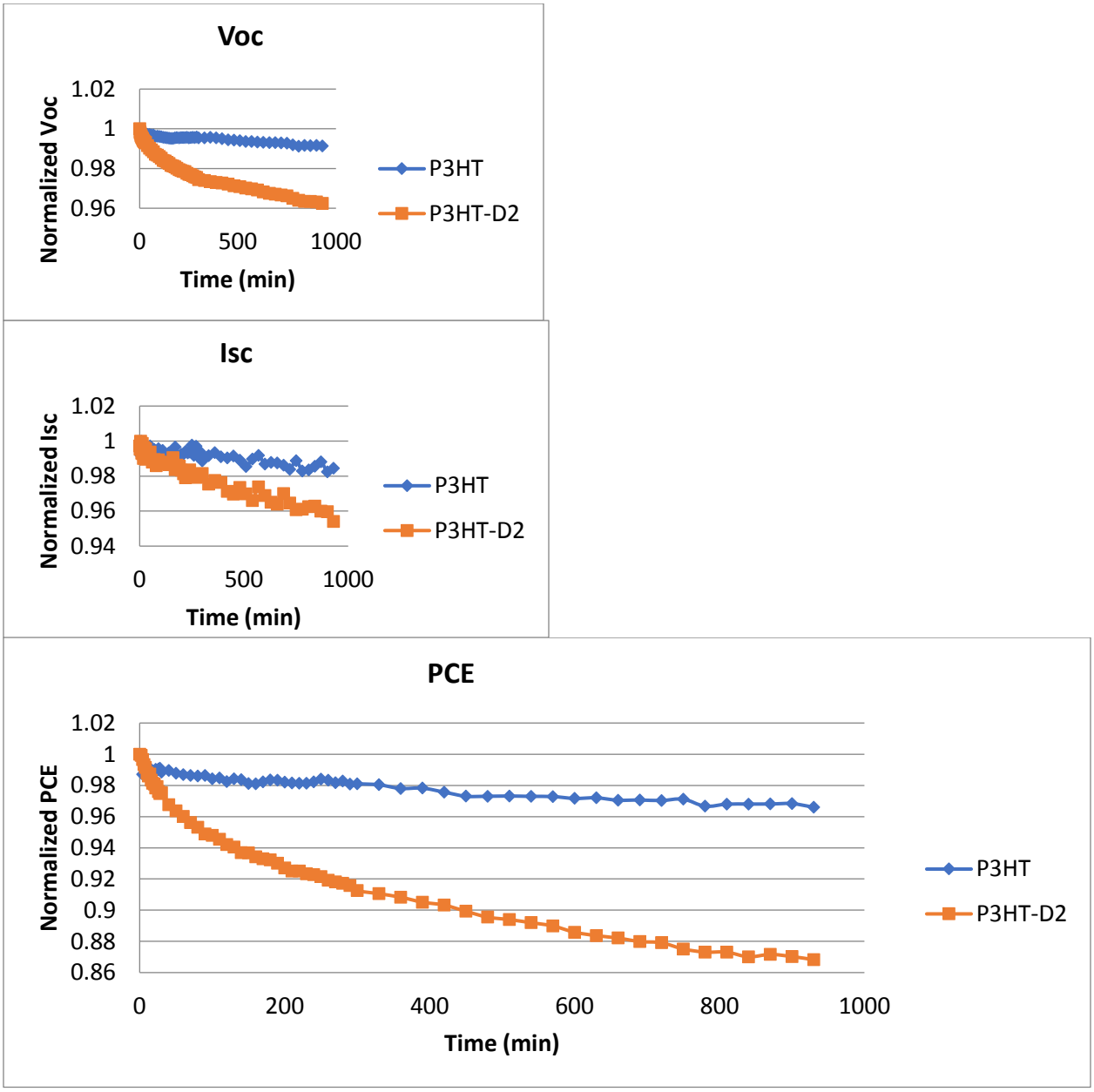

Fig. 8 Comparison of degradation characteristics for P3HT and deuterated P3HT devices

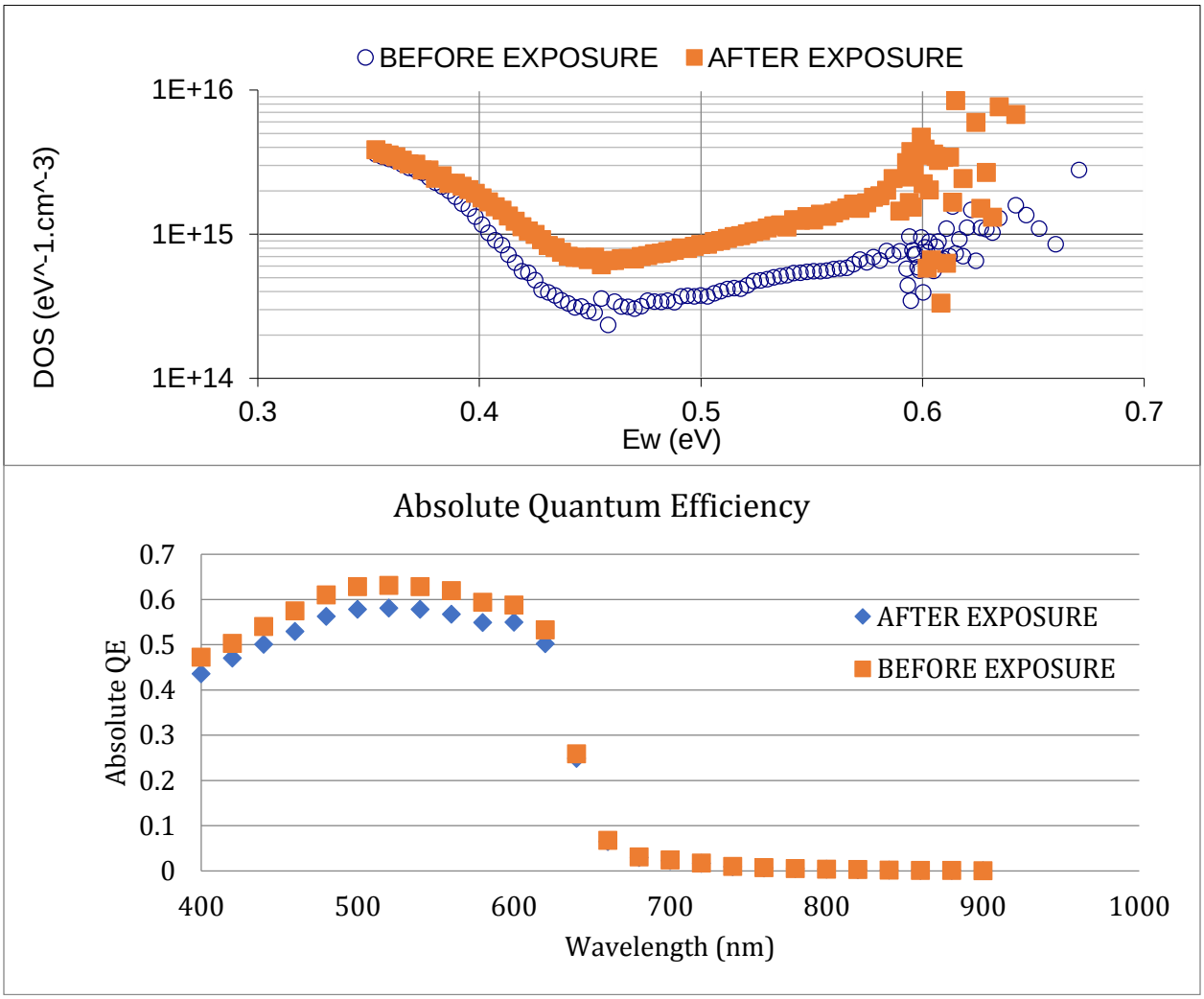

Fig. 9 Comparison of electronic densities of states and quantum efficiencies for deuterated P3HT devices before and after light-soaking

C-F measurements (capacitance-frequency) shows almost a doubling in the density of defect states within the band gap due to 1 day of exposure to 1X Sun intensity.

Absolute quantum efficiency measurements indicate a definite reduction in charge collection efficiency due to degradation. This might be the result of higher charge recombination due to increased defect states within the band-gap.

5.3 Fabrication Method

A solution of P3HT polymer (1-Materials, 17mg) and the organic compound $PC_{61}BM$ (Nano-C, 17mg) in dichlorobenzene (Sigma Aldrich, 1mL) was prepared in an inert atmosphere (glove-box). The solution was stirred at 70°C for 12 hours. ITO coated glass substrates were cleaned thoroughly with surfactant, DI water, acetone, isopropanol and were plasma treated for 10 minutes. PEDOT:PSS (Clevois PVPAI4083) was spin-coated onto ITO/Glass at 4000rpm for 40 seconds and annealed at 150°C for 20 minutes. The samples were then transferred to a glove-box and the P3HT:PCBM solution was spin-coated onto the samples at 400rpm for 60 seconds. The samples were dried for 1.5 hours while covered by a petri dish. Next, the samples were annealed in two steps, first at 160°C for 2 minutes and then at 110°C for 10 minutes. Next, the samples were loaded in a thermal evaporator and calcium (20nm) and aluminum (100nm) were deposited successively to make top electrical contact.

Exactly same procedure was used to fabricate P3HT-d2: PCBM solar cells, replacing only the P3HT polymer with the α-deuterated polymer.

5.4 Degradation procedure

The solar cells were degraded under 1XSun intensity using an ABET solar simulator for 1 day. The light intensity was calibrated using a standard crystalline Silicon solar cell. The degradation was carried out in inert N_2 atmosphere in a glove-box with moisture level less than 1 ppm and oxygen level at a few ppm. This should eliminate any extrinsic degradation. The solar cell device was kept under a fan continuously to eliminate self-annealing effects.

5.5 Procedure for SCLC mobility measurements

SCLC hole mobility was calculated for P3HT and P3HT-d2 polymers using the architecture – Glass/ITO/MoOx/P3HT/MoOx/Au. Molybdenum oxide (20nm) was thermally deposited on ITO/Glass substrates and annealed at 150 °C for 20 minutes. The polymer (P3HT or P3HT-d2) was spin - coated on this sample at 600rpm for 60 seconds. Finally molybdenum oxide (20nm) was again thermally deposited on these samples and annealed at 150 °C for 20minutes. Gold contacts (100nm) were thermally deposited on these samples. The thickness of polymer layers was measured using a profilometer.

CHAPTER 6. LIGHT-MATTER INTERACTION AND PHOTON WAVELENGTH DEPENDENCE OF DEGRADATION IN ORGANIC POLYMER FILMS

6.1 Introduction

In the previous chapters we have described in detail measurements of the degradation of both organic polymer films and organic solar cells utilizing these polymer films in the absorber layer. Light soaking is the critical factor causing the degradation. It is of great interest to understand and characterize the region of the solar spectrum that is causing the degradation process. While it is generally known that short wavelengths in the ultra-violet are especially damaging for organic materials, it is unclear if longer wavelengths (e.g. red/green) also can cause degradation. To this end we examine if there is a minimum wavelength i.e. minimum incident photon energy that is necessary for causing degradation. An important finding in Chapter 2 is that our theoretical calculations predict a minimum energy of ~2.65 eV i.e. 465 nm of photons is necessary to causing O-diffusion in PTB7 polymers, corresponding to blue photons.

To experimentally obtain a measure of the minimum wavelength i.e. minimum incident photon energy that is necessary for causing degradation we perform a systematic experiment of light induced degradation with a sequence of optical filters. We utilize high-pass filters, which allow the transmission of photons above a specified cut-off wavelength (λ_c), with an abrupt cut off of the transmission for wavelengths below the cut-off wavelength. Filters with of 395 nm, 435nm, 475nm, 495 nm, 610nm, 800 nm were acquired from Newport. The wavelength dependent transmission shown in Fig. 1, shows excellent high pass transmission.

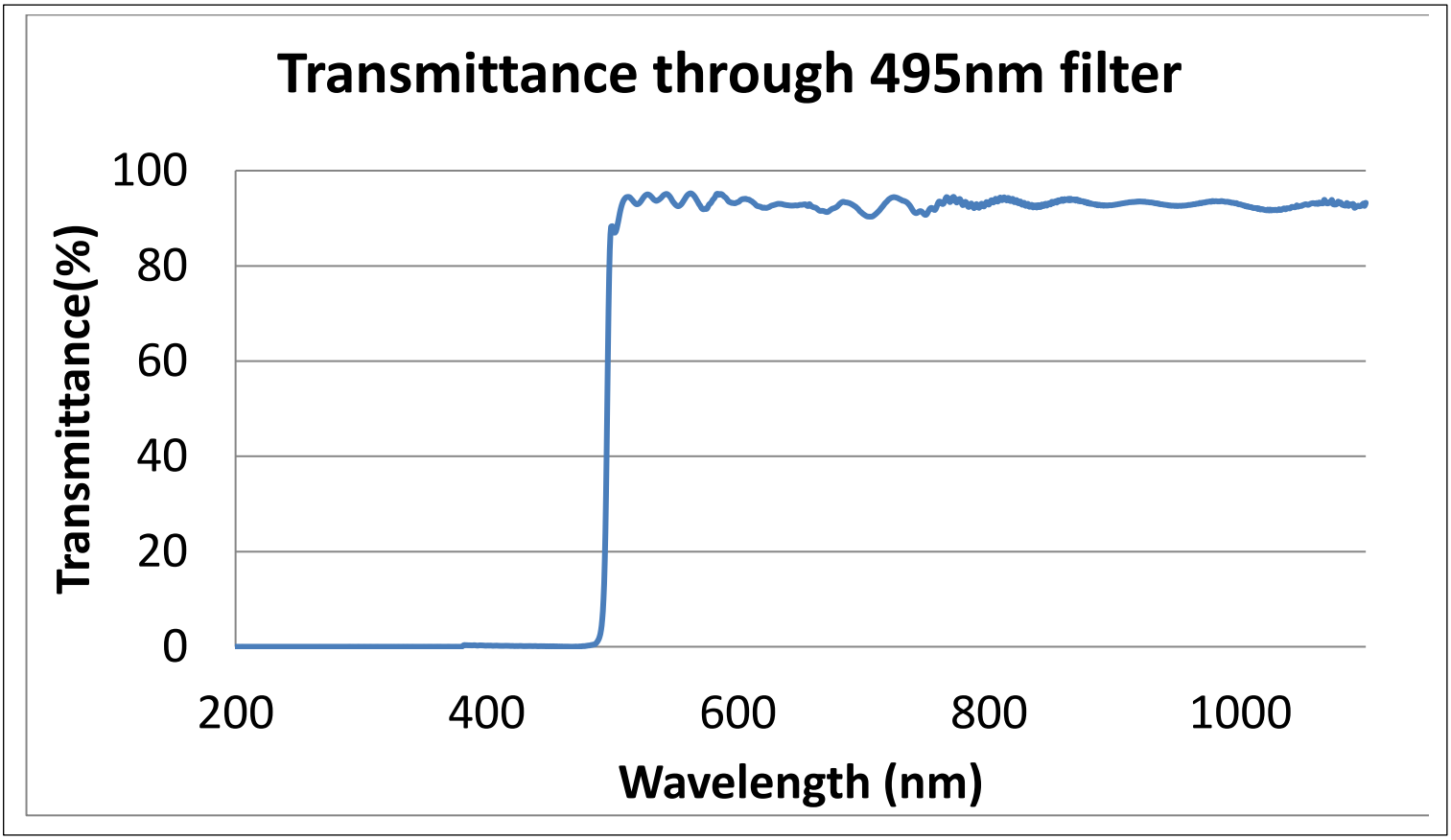

Fig. 1 Transmission as a function of wavelength for a high pass filter with a cut-off wavelength of 495 nm.

6.2 Experimental procedure

Organic polymer films (PTB7:$PCBM_{60}$) were spin coated on sodium chloride substrates at 1000rpm for 60seconds in a glove box with nitrogen atmosphere and moisture level less than 10 ppm. The sample was taken out of glove box in a transfer tube and the FTIR spectrum through the film was immediately measured. Then the film was exposed to 4XSun light passed through a long pass optical filter for 24 hours. This degradation was carried out in ambient room atmosphere with humidity levels ~40-50%. The FTIR through the film was re-measured after this photo exposure to observe differences. This was repeated for optical filters with 6 different cut-off wavelengths.

6.3 Results and Discussion

Without any filters, we expect a general flattening of features in the FTIR spectrum, after degradation in ambient atmosphere, with some increase in 1730cm^{-1} feature, as we saw in detail in Chapter 3. Using the 800nm filter, i.e., blocking all wavelengths below 800nm, the FTIR spectrum (dark blue – bottom most curve) of the degraded film looks very similar to that of the pristine film in both Fig.2 and Fig.3, i.e. high frequency and low frequency curves. With the 610nm filter also, the spectrum is similar to that of pristine film, although we do see two unusual peaks around 2300cm^{-1}. This is likely an artifact from an impurity on the substrate. For the 495nm filter curve we again see a similar FTIR spectrum as the pristine film. However, for 475nm filter curve we see changes in both Fig.2 and Fig.3 – a clear general albeit partial flattening of the curve with the exception of the strong feature at 1730 cm^{-1}. Using the 435nm long-pass filter, we see a complete flattening of the curve both at high and low frequencies. With 395nm filter, i.e., allowing light with wavelengths greater than 395nm, we do see the general flattening of the curve, but with the strong feature at 1730 cm^{-1} similar to what we saw in Chapter 3 for degradation without any filters.

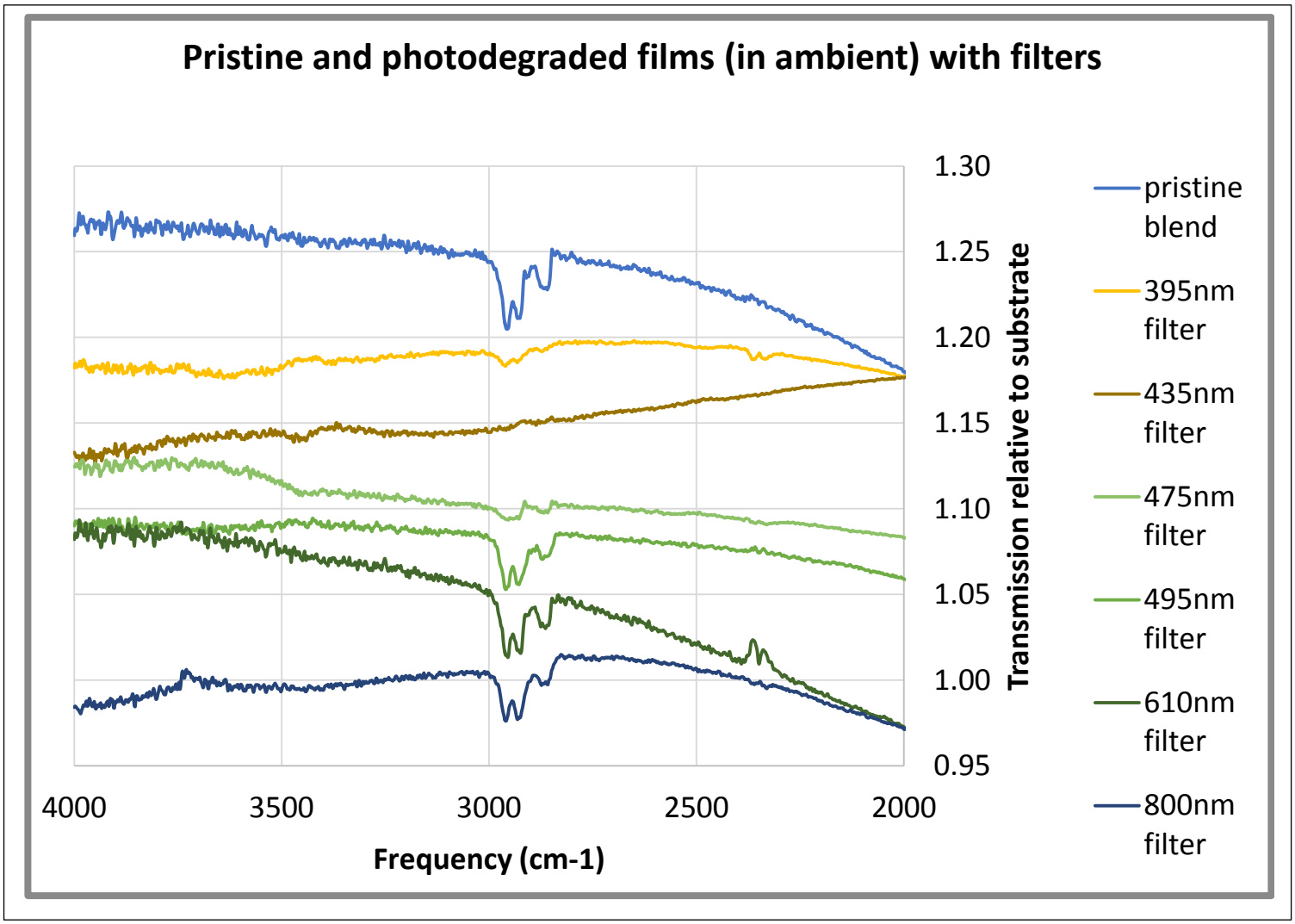

Fig. 2. FTIR spectrum of PTB7:PCBM film between wavelengths 4000 to 2000 cm^{-1} after photo-degradation in ambient atmosphere under 4XSun intensity under different filters. The filters allow light only above a certain wavelength to pass.

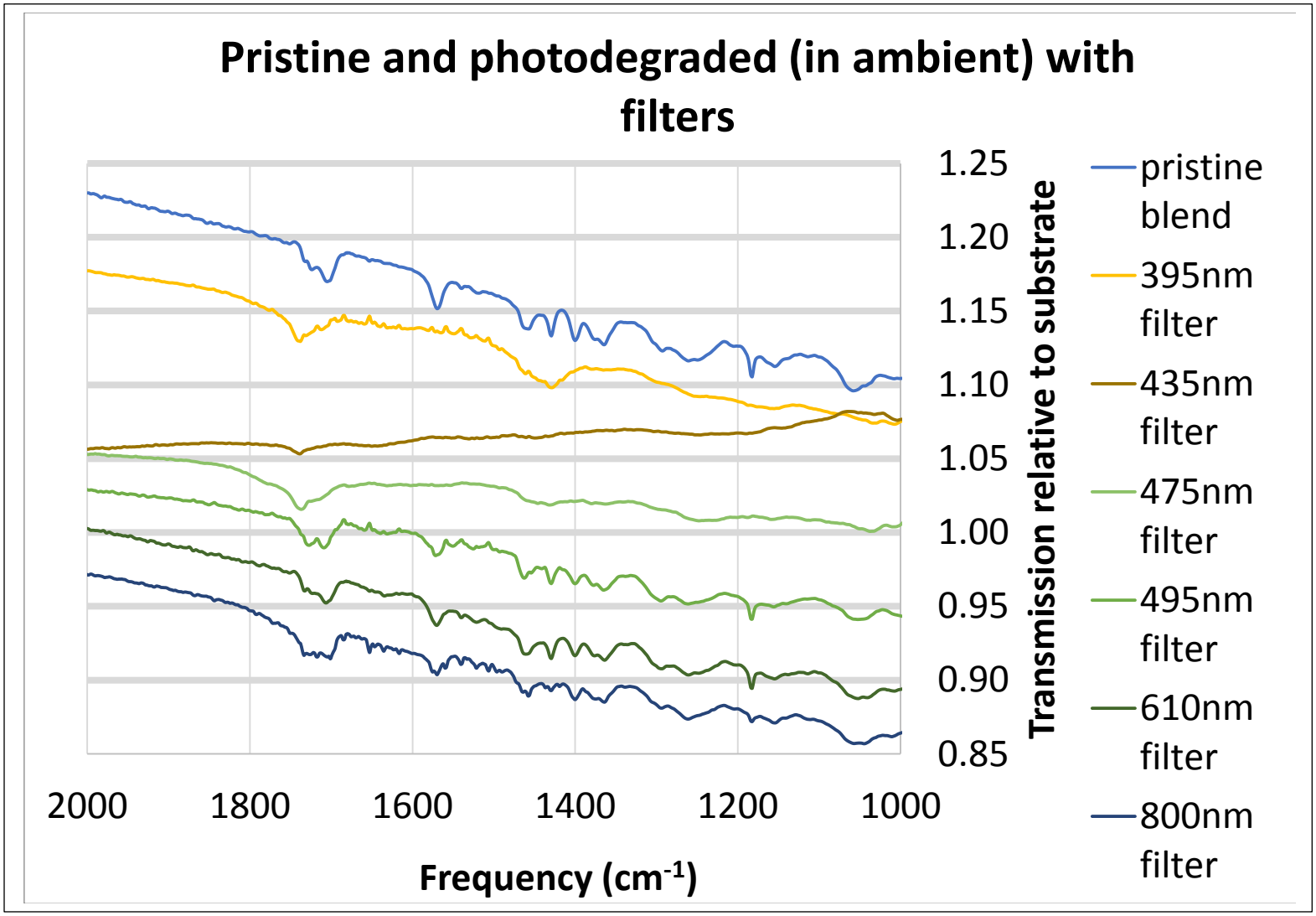

Fig. 3 FTIR spectrum of PTB7:PCBM film between wavelengths 2000 to 1000 cm^{-1} after photo-degradation in ambient atmosphere under 4XSun intensity under different filters. The filters allow light only above a certain wavelength to pass.

6.4 Conclusions

This experiment with optical filters was carried out to estimate the activation energy required for the degradation to occur for PTB7:PCBM organic films. The energy of photons necessary

to change the FTIR spectrum may be regarded as an estimate of activation energy for the photo-degradation reaction. As we see changes in FTIR after photo-degradation for 475nm filter but not for 495nm filter, we can estimate E_a from the energy of 475nm photons, i.e. E_a~2.6 eV. From ab-initio simulations of degradation mechanisms in Chapter 2, we theoretically calculated the activation energy of O-rearrangement photo-degradation reaction to be E_a~2.68 eV (see section 2.4.1). More experiments are needed to establish the correspondence of observed degradation with this reaction mechanism.